The downward influence of stratospheric sudden warmings

PETER HITCHCOCK *

Dept. of Applied Mathematics and Theoretical Physics, University of Cambridge, Cambridge, UK

ISLA R. SIMPSON

Lamont Doherty Earth Observatory, Columbia University, New York, USA

---

*Corresponding author address: Peter Hitchcock, Dept. of Applied Mathematics and Theoretical Physics, Centre for Mathematical Sciences, Wilberforce Road, Cambridge, UK CB3 0WA.

E-mail: aph42@cam.ac.uk

LDEO contribution number XXXX

ABSTRACT

The coupling between the stratosphere and the troposphere following two major strato- spheric sudden warmings is studied in the Canadian Middle Atmosphere Model using a nudging technique by which the zonal mean evolution of the reference sudden warmings are artificially induced in an $\sim$100 member ensemble spun off from a control simulation. Both reference warmings are taken from a freely-running integration of the model. One event is a displacement, the other a split, and both are followed by extended recoveries in the lower stratosphere. The methodology permits a statistically robust study of their influence on the troposphere below.

The nudged ensembles exhibit a tropospheric annular-mode response closely analogous to that seen in observations, confirming the downward influence of sudden warmings on the troposphere in a comprehensive model. This tropospheric response coincides more closely with the lower stratospheric annular mode anomalies than with the mid-stratospheric wind reversal. In addition to the expected synoptic scale eddy feedback, the planetary-scale eddies also reinforce the tropospheric wind changes, apparently responding directly to the stratospheric anomalies.

Furthermore, despite the zonal symmetry of the stratospheric perturbation, a highly zonally asymmetric near surface response is produced, corresponding to a strongly negative phase of the North Atlantic Oscillation with a much weaker response over the Pacific basin which matches composites of sudden warmings from the ERA-Interim reanalysis. The Cou- pled Model Intercomparison Project phase 5 models exhibit a similar response, though in most models its magnitude is under-represented.

1. Introduction

The influence of the stratospheric polar vortices on the position of the tropospheric mid-latitude jets has now been well established by several lines of observational and modeling evidence. In the Northern Hemisphere, the tropospheric zonal mean jet has an observed tendency to shift equatorwards following a weakening of the Arctic stratospheric vortex (Baldwin and Dunkerton 2001, hereinafter BD). Although several possible mechanisms for the downward influence of the stratosphere have been suggested (Haynes et al. 1991; Hartley et al. 1998; Song and Robinson 2004; Wittman et al. 2007; Simpson et al. 2009), their relative importance remains unclear.

The composites of Northern Annular Mode (NAM) anomalies presented by BD remain the most important line of evidence for the shifting of the tropospheric jets following anomalous stratospheric events, and an update of such a composite following major stratospheric sudden warmings is shown in Fig. 1(a). While compelling, such composites raise a number of important questions that remain open. In this study, we focus on the following issues using controlled experiments with a comprehensive general circulation model (GCM):

1. *The downward influence of zonal mean stratospheric variability on the troposphere*

Although the downward tilt present in composites like Fig. 1(a) is visually compelling, Plumb and Semeniuk (2003) demonstrated that it is possible to obtain such apparent downward propagation in a simple model of stratospheric variability in which the anomalies at all levels are demonstrably produced directly by the upward influence from the lower boundary. Moreover, the structure of the circulation anomalies within the stratosphere itself after the wind reversal can largely be explained in a comprehensive model by the vertical structure in radiative timescales (Hitchcock and Shepherd 2013), again requiring no true downward influence.

Sudden warmings are understood to be initiated by waves produced at the surface, which

2

₅₁ will doubtlessly interact with the tropospheric flow directly. The direct influence of these

₅₂ tropospheric anomalies must be controlled for in order to definitively identify the influence

₅₃ of the warmings on the troposphere below. This issue was addressed by Gerber et al. (2009),

₅₄ who strongly perturbed zonal wavenumbers 4 through 10 in the troposphere following several

₅₅ major warmings and demonstrated that the influence of the stratospheric anomalies was

₅₆ apparent in the ensemble mean despite this perturbation of the tropospheric flow. While

₅₇ numerous other simple model studies have demonstrated that changes imposed directly to

₅₈ the vortex can indeed influence the tropospheric jets below (Polvani and Kushner 2002), the

₅₉ forcing imposed on the stratosphere is typically highly idealized or causally distant from the

₆₀ warmings themselves (Haigh et al. 2005; Simpson et al. 2009; Charlton-Perez and O'Neill

₆₁ 2010; Hitchcock et al. 2013b). Zonal asymmetries in the boundary conditions of these models

₆₂ are also simplified or absent, as are parameterizations relevant to the details of the large-scale

₆₃ flow.

₆₄ *2. The separation of the 'deterministic' tropospheric signal from internal variability*

₆₅   The NAM used in the composites in Fig 1(a) (see methods section) has a wintertime stan-

₆₆ dard deviation of ∼1.5. Assuming the 22 events composited in Fig. 1(a) are independent,

₆₇ fluctuations in this composite mean due to internal variability should have a standard devi-

₆₈ ation of $1.5/\sqrt{21} \approx 0.3$. Given that the response is of the order of 0.5 standard deviations,

₆₉ the statistics are marginal at the 95% level of confidence with this number of events, and cer-

₇₀ tainly not sufficient to quantify the exact magnitude or the finer details of the tropospheric

₇₁ response.

₇₂   Issues of statistical robustness are exacerbated by the diversity of stratospheric events

₇₃ and the fact that their influence on the troposphere may itself be quite variable. Gerber

₇₄ et al. (2009) and Hitchcock et al. (2013a) identified the importance of the depth to which the

₇₅ initial warming descends in the stratosphere, with those that descend right to the tropopause

₇₆ producing the most persistent stratospheric anomalies, and the most robust tropospheric

response at long timescales. In particular, it is clear that the Polar-night Jet Oscillation (PJO) events identified by Hitchcock et al. (2013a) exhibit a tropospheric signal that persists substantially longer than the 20 days suggested by Fig. 1(a). In addition, it has been proposed that whether the polar vortex splits in two or is displaced from the pole during the sudden warming is relevant to the subsequent tropospheric evolution (Mitchell et al. 2013), though since splitting events tend to disturb the lower stratosphere more efficiently than do displacements, these two effects must be carefully distinguished.

Marginal statistics are problematic if one is interested in details of the coupling mechanisms. For instance, it is not clear what the time lag between the onset of stratospheric variability and the tropospheric response is. One could argue the relevant timescale is that of the Eliassen adjustment to the rearrangement of stratospheric PV (or the subsequent diabatic adjustment), or that of baroclinic eddy growth rates. The BD composite does not provide a strong observational constraint. While better statistics can now be obtained even from very comprehensive models, details of the tropospheric response vary across models (Gerber et al. 2010, see their Fig. 10), and tend not to be robust either to specifics of the model configuration, or to which criteria are used to define stratospheric events (compare, e.g. Fig. 13 of Hitchcock et al. (2013a) with Fig. 5 below). This suggests the need for a more controlled approach.

3. The zonally asymmetric nature of the tropospheric response

Finally, although the NAM as defined by BD is not zonally symmetric, subsequent studies have used fully symmetric definitions (Baldwin and Thompson 2009) and most simplified modeling studies focus on the zonal mean response (e.g. Polvani and Kushner 2002; Song and Robinson 2004; Simpson et al. 2009; Hitchcock et al. 2013b). Although there are good reasons to do so (for instance, the zonally symmetric response is strongly constrained by the conservation of zonal angular momentum), the composite surface response shown in Fig. 1(b,c) is strongly localized in the Atlantic sector. With the small number of events in

4

the observational record and the large variability in the Atlantic sector, statistical issues pose a challenge for understanding these local responses as well. Again, a controlled approach is needed to identify the robustness of these asymmetries and to further our understanding of the processes responsible.

The approach adopted here to address these three questions is to artificially induce sudden warmings in a comprehensive stratosphere-resolving model by nudging the zonal mean component of the stratospheric circulation towards the time-dependent evolution of a sudden warming, as produced by a free running version of the same model. These ensembles are compared with a control ensemble, produced by nudging the zonal mean in the stratosphere towards the seasonally-varying model climatology. The tropospheric initial conditions of each member are, therefore, fully independent from those that occurred at the onset of the freely simulated warming. Differences in the tropospheric circulation between the two ensemble means are, by construction, due to the downward influence of the nudged circulation.

Furthermore, the zonal mean evolution in the stratosphere in each ensemble member is nearly identical, so any variability within the ensemble is most likely due to variability in the tropospheric dynamics, not due to variability in the zonal mean stratospheric state. Finally, the zonally asymmetric component of the stratosphere is allowed to evolve freely, and can respond to the constrained zonal mean flow. The nudged ensembles do not, however, exhibit the strong asymmetrical displacement or splitting of the stratospheric vortex that occurs during the onset of the reference warmings.

The primary aim of this paper is to establish the methodology and demonstrate the basic features of the model response. The approach of relaxing one component of the general circulation in order to understand its effects on other regions has been applied in several contexts (Alexandru et al. 2009; Bielli et al. 2010; Jung et al. 2010; Hoskins et al. 2012), including that of stratosphere-troposphere interaction (Douville 2009), and the approach used here has recently been applied to isolate the stratospheric contribution to tropospheric annular mode timescales (Simpson et al. 2011, 2013a,b). There are, however, important

5

subtleties associated with the technique and it is not immediately apparent that the response induced by the nudging should be fully analogous to the freely evolving sudden warming. In particular, the nudging amounts to a potential source or sink of angular momentum, which has been shown in other contexts to produce spurious zonally symmetric circulations below the region of relaxation (Shepherd et al. 1996). Nonetheless, it is demonstrated in a companion paper Hitchcock and Haynes (in review, hereinafter HH) that no such spurious circulations are playing a role in the responses seen in these experiments.

Complete details of the methodology and a demonstration that the nudging is indeed achieving its intended purpose are given in section 2. The zonal mean response is presented in section 3, and strongly suggests that the tropospheric signal seen in the BD composites is a result of the downward influence of the stratosphere. Section 4 discusses the response of the eddy fluxes, demonstrating the dominance of the synoptic scale eddy response in the zonal mean but also a non-trivial role for planetary scale eddies. The quasi-stationary, longitudinally dependent, near surface response is shown in section 5, and discussion and conclusions are then given in section 6.

2. Methodology

a. Model Experiments

The experiments were performed with the Canadian Middle Atmosphere Model (CMAM), a comprehensive GCM (Scinocca et al. 2008) run at T63 spectral truncation and 71 vertical levels with a model top at 0.0006 hPa (roughly 100 km). All integrations were carried out with climatological repeated annual cycle sea-surface temperatures and sea-ice (collectively, SSTs). The greenhouse gases and SSTs are held fixed at levels representative of 1990, and a climatological ozone field is specified, all as described in the 'DYN-MAM' configuration of Scinocca et al. (2008).

Three sets of experiments will be discussed: a free running, 100-year time-slice integra-

tion (FREE), a 100-year time-slice integration (CTRL), in which the zonal mean state of the stratosphere is constrained to the climatology of FREE, and finally, two 100-member ensembles of integrations (SSW) spun off from CTRL in which the zonal mean state of the stratosphere is constrained to follow the evolution of a specific reference stratospheric sudden warming simulated by FREE.

The control run CTRL has been constrained by applying an additional relaxation on the zonal-mean spectral components X of the temperature, vorticity, and divergence fields of the form $-K(p)(X - X_0)/\tau_N$, where the reference state X_0 is the climatology X_c of the respective field from FREE, τ_N is 6h, and $K(p)$ is a height dependent pre-factor which varies between 0 and 1. The relaxation is applied only in the stratosphere, with a $K(p)$ that is 0 from the surface up to 68 hPa, rises linearly to 1 at 28 hPa, and remains at 1 above. Strictly speaking the nudging is performed on model hybrid-pressure levels, but at these levels the difference between the model levels and pressure surfaces is small. The zonally-asymmetric components are allowed to evolve freely. FREE and CTRL have also been analyzed by Simpson et al. (2011, 2013a,b) and more details can be found therein, but note that CTRL was termed NUDG.

The goal of each SSW ensemble is to constrain the zonal mean evolution of the stratosphere to follow that of a particular stratospheric sudden warming, while permitting the troposphere and the stratospheric eddies to evolve freely in response. They are performed by initializing a new experiment from a boreal winter reference date each year of the CTRL run. In each member, a relaxational term of the same form as above is applied, but here the reference X_s is taken to be the instantaneous state of a specific sudden warming that occurred in FREE.

The stratospheric variability in FREE has been described in detail by Hitchcock and Shepherd (2013), who found it to have statistics in good agreement with observations. Two sudden warmings have been chosen as reference cases for the SSW ensembles: the displacement event in late December of model year 17, and the split event in late December of model

7

182 year 93 (see Fig. 1 of Hitchcock and Shepherd (2013)). The cases based on the displacement

183 and split reference events will be referred to as SSWd and SSWs, respectively.

184   In order to isolate the impact from the sudden warming itself (as opposed to any precon-

185 ditioning of the stratosphere that may have occurred prior to the warming), the reference

186 date on which these integrations begin is chosen to be 21 December, such that the instan-

187 taneous state of FREE during the reference case for both SSWd and SSWs was reasonably

188 close to X_c. The remaining discontinuity, though small, does complicate the study of the

189 initial adjustment. In the reference year for SSWs, a second stratospheric wind reversal

190 occurs in mid-March. This secondary event is classified as a sudden warming by the Charl-

191 ton and Polvani (2007) criteria, but was excluded in Hitchcock and Shepherd (2013) by the

192 McLandress and Shepherd (2009) requirement that wind reversals be separated by at least

193 60 days. Both primary events are examples of Polar-night Jet Oscillation events (Hitchcock

194 et al. 2013a), characterized by their associated lower stratospheric temperature anomalies

195 that persist for several months. These events are responsible for the persistence seen in the

196 BD composites (Hitchcock et al. 2013a), and as such are of particular interest for the cou-

197 pling to the troposphere and for their potential contribution to conditional skill in seasonal

198 forecasting (Sigmond et al. 2013). The secondary event in SSWs also shows persistent strato-

199 spheric temperature anomalies, but was not formally classified as a PJO event by Hitchcock

200 and Shepherd (2013) due to their relatively weak amplitude. Since both primary events

201 occurred in late December, these experiments cannot speak to the seasonal dependence of

202 the tropospheric response.

203 *b. The influence of the nudging*

204   The nudging technique can be seen to reproduce the zonal mean circulation of the ref-

205 erence events in Fig. 2, which shows the zonal mean zonal wind anomalies at 60°N of the

206 FREE events and the SSW ensembles. The stratospheric evolution in the SSW ensembles

207 is clearly reproducing that of the freely simulated reference events. The secondary event

₂₀₈ beginning in mid-March in the SSWs case is apparent.

₂₀₉ As stressed above, no relaxation is applied directly to the stratospheric eddies. There is,
₂₁₀ therefore, no guarantee that the wave driving in the SSW ensembles will match that in the
₂₁₁ freely simulated events, particularly during the onset of the warming. The tropospheric state
₂₁₂ in each ensemble member is fully independent from the tropospheric state that produced the
₂₁₃ warming in FREE, and even if the amplification of the waves in the FREE case was due
₂₁₄ to resonance (Matthewman and Esler 2011, and references therein), the stratospheric state
₂₁₅ in the nudged ensembles is constrained to be close to climatology until the onset of the
₂₁₆ warming, allowing little time for the waves to amplify.

₂₁₇ The time series of Eliassen-Palm (EP) flux divergence, integrated vertically from 100 hPa
₂₁₈ to 1 hPa, is shown for the SSWd case in Fig. 3. All EP-fluxes and associated Transformed-
₂₁₉ Eulerian Mean (TEM) quantities are computed for the primitive equations on log-pressure
₂₂₀ coordinates as described in Andrews et al. (1987). As expected, the initial pulse of high-
₂₂₁ latitude wave driving that drives the wind reversal at 10 hPa (roughly from 25-30 Dec in
₂₂₂ the FREE simulation is not reproduced by the SSWd ensemble. Neither is the second pulse
₂₂₃ in late January which produces the lower stratospheric anomalies in FREE. Although the
₂₂₄ accelerations associated with the second pulse are smaller than the initial pulse, they occur
₂₂₅ at lower altitudes (though still predominantly within the nudging region), and so contribute
₂₂₆ more to the mass-weighted divergence in Fig. 3(a).

₂₂₇ This anomalous wave activity represents sources and sinks of angular momentum within
₂₂₈ the stratosphere that the nudging must produce to constrain the stratospheric evolution
₂₂₉ to the reference events. This non-conservation of angular momentum has been shown to
₂₃₀ disrupt the 'downward control' mechanism (Shepherd and Shaw 2004), and so it is essential
₂₃₁ to understand the effects of the zonally-symmetric nudging on the meridional circulation.
₂₃₂ This problem is considered in detail by HH; and indeed within the nudging region itself
₂₃₃ there are significant differences in the meridional circulation, driven by differences in the
₂₃₄ stratospheric wave driving between the SSW ensembles and the reference events in FREE

9

₂₃₅ (see their Fig. 8). However, it is shown by HH that the diabatic effects of the nudging act

₂₃₆ to confine this anomalous circulation within the nudged region, and thus below the level of

₂₃₇ the nudging, the residual circulation (and thus the associated Coriolis force and adiabatic

₂₃₈ heating) induced by the nudging will very closely resemble that produced by the stratospheric

₂₃₉ forcing in the freely simulated stratospheric event.

₂₄₀ To demonstrate that the tropospheric Coriolis accelerations are indeed reproduced suf-

₂₄₁ ficiently well in the nudged ensemble, Fig. 4 shows the anomalous Coriolis acceleration

₂₄₂ induced at 700 hPa by the stratospheric wave-driving (both resolved and parameterized) for

₂₄₃ the FREE displacement event and by the wave-driving and nudging in the SSWd ensemble

₂₄₄ (see, e.g. (7) of HH). This is computed using a zonally symmetric quasi-geostrophic model

₂₄₅ on the sphere; details of which are given in the appendix. The details of the influence of the

₂₄₆ stratospheric forcings in the reference event (Fig. 4(a)) are well reproduced by the nudging

₂₄₇ in the SSWd ensemble (Fig. 4(b)). The difference (Fig. 4(c)) is most apparent through early

₂₄₈ January when the difference in the wave driving is strongest (Fig. 3(c)).

₂₄₉ A second issue arising from the presence of the strong nudging region that is identified

₂₅₀ and quantified by HH is the presence of a spurious feedback analagous to the 'sponge-layer'

₂₅₁ feedback described by (Shepherd et al. 1996), that affects the region about a scale-height

₂₅₂ below the nudging layer. The strength of this feedback is closely related to the strength of the

₂₅₃ confinement of the anomalous residual circulation within the nudged region, but produces

₂₅₄ only weak spurious effects at the intraseasonal timescales of interest in the present work.

₂₅₅ We can expect, therefore, that any coupling induced through (a) the mean meridional

₂₅₆ circulation or through (b) the response of tropospheric eddies to lower stratosphere pertur-

₂₅₇ bations will be active and well represented in the SSW ensembles. On the other hand, the

₂₅₈ zonally asymmetric circulations in the stratosphere associated with the vortex displacement

₂₅₉ or the vortex split are not present, and therefore mechanisms dependent on this stratospheric

₂₆₀ zonal asymmetry will not be active. Furthermore, since the pulses of planetary waves that

₂₆₁ produce the sudden warming in the FREE run are not present in the nudged ensembles by

10

₂₆₂ construction, the tropospheric torques arising from these initial pulses of wave activity will
₂₆₃ be missing from the nudged ensembles and will not be responsible for any tropospheric sig-
₂₆₄ nal seen. Any two-way wave coupling (Shaw et al. 2014) present in the nudging run cannot
₂₆₅ involve these pulses.

c. *Data and Indices*

₂₆₇ The composites shown in Fig. 1 are computed from the ERA-Interim reanalysis product
₂₆₈ (Dee et al. 2011) using daily geopotential heights, 10hPa zonal wind, 2m temperature and
₂₆₉ 10m zonal and meridional wind fields for November through March (NDJFM) from the 33
₂₇₀ winters between 1979/1980 and 2011/2012. In section 5, composites of near surface fields
₂₇₁ following sudden warmings are shown for the Coupled Model Intercomparison Project, phase
₂₇₂ 5 (CMIP-5) multi-model data set. For CMIP-5 we make use of the daily 10hPa zonal wind,
₂₇₃ surface temperature (tas) and surface zonal (uas) and meridional (vas) wind fields for the
₂₇₄ NDJFM seasons of the "historical" simulations from 1960/1961 to 2003/2004. The models
₂₇₅ and ensemble members used are summarized in table 1.

₂₇₆ The Northern Annular Mode (NAM) is defined here to be the first, area-weighted, EOF
₂₇₇ of de-seasonalized zonal mean geopotential heights north of the equator on each pressure
₂₇₈ level, following Baldwin and Thompson (2009). It is, as a result, purely a feature of the
₂₇₉ zonally averaged circulation. The EOF is defined using all days of the FREE simulation.
₂₈₀ The NAM indices for the SSW ensembles and CTRL are then computed by projecting the
₂₈₁ daily geopotential height anomalies (from the climatology of CTRL) onto this structure.
₂₈₂ The North Atlantic Oscillation (NAO) is defined as the first (area weighted) EOF of surface
₂₈₃ pressure in the region 90° W to 40° E, 20° N to 80° N in the FREE simulation and the NAO
₂₈₄ index in other runs is again calculated by projecting the monthly mean surface pressure
₂₈₅ anomalies (also from the climatology of CTRL) onto this structure.

₂₈₆ Stratospheric sudden warmings are defined following Charlton and Polvani (2007). For
₂₈₇ ERA-Interim, 22 events were obtained in the 33 winters considered using this criterion. For

11

CMIP-5, only those models for which there were at least 10 sudden warming events in the historical simulations were included to ensure some robustness of the sudden warmings composite anomalies. There were 24 models that provided the necessary data to perform this composites and of these 24, only 16 had at least 10 events by this criterion (Table 1). This is confirmation that GCMs, in particular those with a low top, tend to underestimate stratospheric variability (Charlton-Perez et al. 2013). The composite average for each individual model was first obtained before taking the multi-model mean.

3. Zonal Mean Response

a. Annular mode response

We consider first the zonal mean response of the troposphere in each SSW ensemble. Time-height plots of the NAM in FREE are shown in Figs. 5(a) and (c). The evolution of the corresponding SSW ensemble mean NAM index is shown in panels (b) and (d). The stratospheric evolution in the SSW ensembles matches that of the reference events, though the correspondence is not as strong as in Fig. 2. This is because, unlike the zonal wind, the NAM is a vertically integrated measure of the circulation, influenced by surface pressure and temperature variability below the level of the nudging (Mudryk and Kushner 2011). The SSW ensembles reproduce a strong response well below the level of the nudging with a magnitude that decreases markedly near the tropopause.

In both ensembles there is a statistically significant tropospheric response, reaching just over one standard deviation in the mid-troposphere with a slightly stronger response near the surface (note that the amplitude of the NAM EOFs also decreases towards the surface). Over the evolution of the SSW ensembles, the largest tropospheric NAM response occurs nearly simultaneously with the largest NAM anomalies in the lower stratosphere. For example, in SSWd, the lower stratospheric anomaly strengthens only in early February, nearly a month after the wind reversal at 10 hPa. It persists for two months, until the end of

12

³¹³ March, throughout which the tropospheric response is evident. In the SSWs case, the lower

³¹⁴ stratospheric anomaly strengthens in early January, about 15 days after the wind reversal,

³¹⁵ as does the tropospheric NAM. In contrast, the stratospheric NAM anomaly strengthens

³¹⁶ throughout the stratosphere simultaneously during the onset of the second warming in mid-

³¹⁷ March. The tropospheric response coincides well with the lower stratospheric anomaly,

³¹⁸ persisting to late April.

³¹⁹   Figure 5(e) shows a composite of the NAM index over all sudden stratospheric warmings

³²⁰ as defined by the Charlton and Polvani (2007) criteria in the FREE simulation, from 30

³²¹ days prior to the stratospheric wind reversal, to 150 days following. In contrast to the two

³²² reference events, there is no delay between the wind reversal and the lower stratospheric

³²³ NAM anomaly in the composite, indicating that this delay is not a universal characteristic

³²⁴ of events in this simulation. It has been argued that this type of delay is more characteristic

³²⁵ of displacements than of splits (Matthewman et al. 2009; Hitchcock et al. 2013a) as a result

³²⁶ of the potentially larger role for the barotropic mode in the latter; the delay during the split

³²⁷ case is indeed shorter than that seen during the displacement case. In the composite there

³²⁸ is also a weak signal in the troposphere prior to the stratospheric wind reversal, which is

³²⁹ not present in the SSW ensembles by experimental design. These issues of the timing aside,

³³⁰ the vertical structure of the NAM response in the SSW ensembles closely resembles that in

³³¹ the composite mean. The amplitude of the composite is weaker than the SSW ensembles

³³² (by about a factor of 2); this is to be expected since the composite includes all sudden

³³³ warmings regardless of whether they are followed by a PJO event (Hitchcock et al. 2013a,

³³⁴ see their Fig. 13), and the reference events chosen for the nudging experiments are large

³³⁵ amplitude examples. The relative strengths of the lower stratospheric anomaly and the

³³⁶ tropospheric signal, as well as the persistence of the latter, agrees well between the ensemble

³³⁷ and composite means.

³³⁸   The nudged, zonal-mean stratospheric anomalies associated with the reference events

³³⁹ produce an ensemble-mean tropospheric annular mode response that strongly resembles the

signal following sudden warmings produced by the freely running model. Therefore, we may consider the SSW ensemble response to be representative of the response to similar magnitude events in the free running model or, indeed, the real world.

The variability of the tropospheric response is addressed in Fig. 6. Figure 6(a) shows histograms of the daily NAM indices at 500 hPa in January through March for the two SSW ensembles and CTRL. The negative NAM seen in the ensemble average is a result of a uniform shift of the distribution towards negative values: little change in the variance is seen. The likelihood of extreme negative NAM events is substantially increased: the fraction of days with a 2σ negative NAM anomaly is 4.4% in CTRL and increases to 11.9% in SSWs and 13.2% in SSWd. Since the variability around the ensemble mean does not change, these histograms are consistent with the characterization of the stratospheric influence as simply biasing the mean state of the tropospheric annular modes (Simpson et al. 2011; Sigmond et al. 2013).

This is further borne out by considering the autocorrelation function of the NAM during DJFMA. Figure 6(b) shows the autocorrelation function at 500 hPa for the FREE run, for CTRL, and for the two SSW ensembles. In the case of the latter two, the autocorrelation is computed from anomalies from the ensemble mean. The autocorrelation function in the SSW ensembles closely match that of CTRL. The serial correlations are somewhat stronger in the FREE run, consistent with the influence of stratospheric variability (Simpson et al. 2011). This holds at other tropospheric levels as well (not shown).

The character of the variability within the ensemble is further illustrated in Figs. 6(c,d) which show the 500 hPa annular mode time series for each member of the SSWd and SSWs ensemble, respectively. The time evolution of the ensemble mean response is shown, with 95% confidence intervals for 22-member sub-samples and the full 100-member ensemble. The 22-member confidence interval agrees well with the rough estimate of 0.3σ given in the introduction. The 100-member confidence interval is small enough to conclude that the finer scale temporal features of the response are in the ensemble mean and therefore reflect

14

the response to the details of the particular stratospheric circulation that occurred in the reference runs.

b. Non-annular mode response

In addition to the NAM response, the full, zonal-mean, tropospheric response in the SSW ensembles shows some further latitudinal structure (Fig. 7). The connection of the tropospheric wind anomalies with lower stratospheric temperatures is confirmed by the strong correlation between the 500 hPa wind anomalies and the 200 hPa temperature anomalies near the pole. The projection of the reponse on to the 1st EOF of zonal wind variability in the FREE run is shown in Fig. 7(c) and (d), and the difference between the full field and the projected anomalies are shown in Fig. 7(e) and (f). There is a high latitude response that does not project on to the leading EOF in both cases for several weeks following the wind reversals (including the secondary event in SSWs). This response arises before the annular mode response. The non-annular mode response more closely resembles the meridional structure of the Coriolis term shown in Fig. 4(b), though a more quantitative analysis that is beyond the scope of the present work is required to say definitively whether it can be attributed to the Coriolis term itself. The meridional structure of the non-annular mode response does not correspond to the second EOF (which describes a broadening or narrowing of the mid-latitude jet). It is apparent at all tropospheric levels, and is robust to the use of a seasonally-dependent annular mode structure in the troposphere.

4. Response of the eddy fields

A key feature of the extended recoveries that characterize PJO events such as the two reference events considered here is the suppression of planetary waves entering the vortex in the months following the sudden warming. Figure 8 shows the difference in planetary-scale (zonal wavenumbers 1 to 3) vertical EP fluxes, averaged from 50 to 90 N between the SSW

ensembles and the control. Like in the PJO event composites of Hitchcock et al. (2013a), the planetary wave driving is suppressed in the vortex following the warming. The suppression extends down into the troposphere below. While this suppression must ultimately arise in the SSW ensembles from the imposed zonal mean stratospheric circulation anomalies, it is unfortunately not possible to attribute this suppression directly to the stratospheric circulation on the basis of experimental design alone, since the tropospheric circulation changes systematically as well.

We turn now to the tropospheric eddy fluxes in the SSWd ensemble, though the response of SSWs is similar. The top row of Fig. 9 shows the planetary scale EP fluxes averaged over January through March from the CTRL run, as well as the zonal mean zonal wind. The climatological vertical fluxes maximize near the surface at 50°N, significantly north of the maximum in the surface westerlies. Much of the flux turns equatorwards into the upper-tropospheric jet to the south of this maximum. The second row of panels show the anomalous fluxes during the first 15 days of the SSWd ensemble, when the high-latitude winds have responded, but preceding the strong annular mode response. The high-latitude suppression of vertical fluxes seen in Fig. 8 is already apparent at this phase, and is accompanied by an increase in vertical fluxes to the south of the climatological maximum, though this lower latitude increase does not extend into the stratosphere (not shown). This pattern amplifies through February of the SSWd ensemble (Fig. 9(e,f)), during which the zonal mean tropospheric response more closely resembles the annular mode.

To compare these responses to the eddy flux perturbations associated with the internal tropospheric variability, Fig. 9(g,h) shows the eddy flux fields from FREE regressed (as a function of latitude and pressure) against the NAM index at 300 hPa, scaled by the anomalous NAM at 300 hPa in the SSWd ensemble (Fig. 5(b)) averaged over February and March, so their amplitudes are comparable to the signals just discussed. The wind anomalies (computed similarly) associated with the NAM for the most part resemble the FM response, although there are some differences in the lower troposphere at high latitude. The

16

⁴¹⁸ meridional fluxes associated with the NAM variability also match the response. However,
⁴¹⁹ the high-latitude reduction in the vertical fluxes apparent in Fig. 9(e) are not a feature
⁴²⁰ of the NAM variability, suggesting that this suppression is a response to the stratospheric
⁴²¹ circulation anomalies. It is also unlikely that this is a response to the lower-tropospheric
⁴²² wind anomalies that are not present in the NAM variability, since similar regressions using
⁴²³ an index based on the structure of wind response in Fig. 9(e,f) also fails to reproduce this
⁴²⁴ suppression. Similar structures are obtained if the regression is performed against the NAM
⁴²⁵ at other levels in the troposphere, or if the CTRL variability is used. One possible mechanism
⁴²⁶ for this reduction in the vertical fluxes is enhanced reflection from the stratosphere (Shaw
⁴²⁷ et al. 2014), though as noted by Hitchcock et al. (2013a), the upper stratospheric shears
⁴²⁸ at this point are strongly positive, which is in the opposite sense of that suggested to be
⁴²⁹ required by the index of Perlwitz and Harnik (2004). Another possibility is that barotropic
⁴³⁰ modes Matthewman and Esler (2011) that can normally be excited by the topography are
⁴³¹ simply not present in this stratospheric configuration.

⁴³² Similar plots for the tropospheric EP-fluxes for higher zonal wave numbers (4 and above)
⁴³³ are shown in Fig. 10. In contrast to the planetary scales, the maximum in near-surface
⁴³⁴ vertical fluxes coincides with the maximum in surface westerlies, as expected. The initial,
⁴³⁵ non-annular mode phase of the SSWd ensemble shows a very weak response in the vertical
⁴³⁶ fluxes, and a reduction of the upper tropospheric equatorward flux of a similar magnitude to
⁴³⁷ that seen at planetary scales. In contrast, the response of these eddies during the annular-
⁴³⁸ mode phase is substantially stronger than the planetary scale response, with a clear dipolar
⁴³⁹ response in the vertical fluxes that aligns with the dipolar wind response and a decrease in
⁴⁴⁰ the meridional flux of 20 to 30% of the fluxes in the control run. These anomalous fluxes
⁴⁴¹ dominate those of the planetary-scale meridional fluxes at this point in the response. Unlike
⁴⁴² the planetary scale fluxes, features of both the meridional and vertical fluxes closely resemble
⁴⁴³ anomalies associated with the NAM itself.

⁴⁴⁴ It is clear that the synoptic scale eddy feedback identified by Polvani and Kushner (2002)

17

plays a large role in the zonal mean annular mode response. The tropospheric planetary scales, however, are also responding significantly with a distinct meridional and temporal signature. The role of the planetary-scale fluxes in this response was identified by Song and Robinson (2004), and has been discussed recently by Hitchcock et al. (2013b); Domeisen et al. (2013); Martineau and Son (2013). Unlike the synoptic scale fluxes, at least the vertical flux anomalies appear to be a direct response to the stratospheric anomalies themselves.

5. Zonally asymmetric response

As discussed in the introduction, composites of observed sudden warmings in the reanalysis show strong zonal asymmetries at the surface. The 2m temperature anomalies and 10m zonal wind anomalies are shown averaged over January and February for SSWs in Figs. 11(a-d) and SSWd in Figs. 11(e-h). Despite the absence of strong displacement or splitting of the stratospheric polar vortex during the onset of the warming in the nudged ensembles, a zonally asymmetric surface response emerges. Comparison of February with January reveals, for the most part, broadly similar temperature and wind anomaly patterns but with an amplified magnitude in February. Regions where this is not true are in the Pacific, where the location of the maximum zonal wind anomaly differs slightly and over the east coast of the US, where the temperature anomalies change sign from January to February.

When compared with the ERA-Interim composites (Figs. 1(b,c)), the ERA-Interim composites are noisier, because fewer warmings are considered, but there is a remarkable similarity. In both cases, the response closely resembles a large amplitude, negative NAO anomaly. The equatorward shift of the mid-latitude circulation that is seen in the zonal mean in response to the stratospheric events is in fact strongly zonally asymmetric. A large equatorward shift occurs in the Atlantic sector in both CMAM and ERA-Interim, whereas in the mid-latitudes of the Pacific the surface wind response is very weak in ERA-Interim and the agreement with the nudged ensembles is less robust.

18

⁴⁷⁰ Although the SSTs are prescribed in the nudged ensembles, the near-surface wind anomalies over the Atlantic basin are likely sufficiently persistent and large-amplitude to make a significant impact on the ocean circulation (Reichler et al. 2012).

⁴⁷³ Referenced against the reversal of the 10 hPa winds, the January response in the SSW ensemble corresponds more directly to the 30 days following the warmings used in the ERA-Interim composite. However, referenced against the lower stratospheric anomalies it may be more appropriate to compare the ERA-Interim composite with the February signal in the SSW ensembles. Since the spatial patterns do not differ strongly, this is primarily an issue for comparisons of the magnitude of the response.

⁴⁷⁹ There are three prominent regions where substantial temperature anomalies occur in the SSW ensembles and where the response is in agreement with the ERA-Interim composite. Firstly, a substantial warming occurs over western Greenland, eastern Canada and the Labrador sea. This warming is around 2K in ERA-Interim and up to 4K in February of the nudged SSW runs. Secondly, a substantial cooling is produced over Northern Europe and Siberia which is of the order of 2K in the 30 days following the stratospheric events in both ERA-Interim and January of the CMAM nudged runs but reaches 4K in February of the nudged runs. Finally, the SSW ensembles also show a substantial warming over North Africa and the Middle East. This warming in ERA-Interim is stronger than occurs in the January of the nudged run but by February it is of comparable magnitude.

⁴⁸⁹ The close resemblence between the surface response in the CMAM nudged warmings and that in the ERA-Interim composite is remarkable given that

• In the nudged run, only the zonal mean component of the warming has been imposed whereas the warmings in ERA-Interim have considerable zonal asymmetry to them with some being vortex splits and some being vortex displacements.

• In the CMAM nudged run we deliberately chose a warming that was characterized by a very long timescale recovery in the lower stratosphere, whereas the ERA-Interim

19

composite is averaging over all different "flavours" of sudden warming, including those with much shorter timescales (Hitchcock et al. 2013a).

- The CMAM nudged events all occur in January, whereas the events in the ERA-Interim composite occur throughout the winter season.

- Climatological SSTs are prescribed in the ensembles and so the ability of near surface temperatures to change over the ocean is restricted.

This provides strong evidence that the temperature anomalies over Greenland, Eastern Canada and the Labrador sea, North Africa and the middle east and Northern Europe and Siberia as well as the equatorward shift of the Atlantic jet are indeed a robust response to the stratospheric anomalies during a sudden warming.

To emphasize the magnitude of this surface response, histograms of the monthly averaged NAO state in the two SSW ensembles and in the CTRL run are shown in Fig. 12. As with the NAM histograms (Fig. 6(a)), the change in the distribution is consistent with a shift of the mean, though the use of monthly averages makes the histograms noisier. The shift in the mean, which exceeds 1 standard deviation in both SSW ensembles, is larger than the shift in the daily NAM indices. The change in frequency of large negative monthly NAO events is even more pronounced than for the daily NAM; the frequency of a -2σ monthly mean event is 1.3% in CTRL, and increases to 13.5% in SSWs and 16.2% in SSWd.

Since the structure of this response is remarkably robust in the ERA-Interim composite and the two SSW ensembles, it is worth asking whether the CMIP-5 models behave similarly. The multi-model mean composites for the CMIP-5 models (described in Table 1) are shown in Fig. 13(a) and (b). Qualitatively similar structures to those in the CMAM nudged run and in ERA-Interim are found with a warming centered over the Labrador sea, a cooling over Northern Europe and Siberia and warming over North Africa and the Middle East. These anomalies, again, accompany an equatorward shift of the Atlantic jet. The magnitude of the anomalies (shown for three regions in Fig. 13(c)), however, particularly over

20

the Labrador sea, are considerably reduced from those in ERA-Interim and in the CMAM nudged run. This is equally true of high-top models as it is of low-top models (following the classification of Charlton-Perez et al. (2013)) which produce sudden warmings. This deficiency warrants further investigation, in particular, as to whether this is a result of a poor representation of deeply penetrating, long timescale stratospheric variability or whether the model troposphere's don't respond as strongly to similar SSW events.

6. Conclusions

A nudging technique has been introduced in order to efficiently produce a large ensemble of sudden warming analogues in a comprehensive stratosphere-resolving GCM. This is achieved by spinning off simulations from a long control run every December, and relaxing the stratospheric zonal mean state towards that obtained during a reference sudden warming, produced by a free-running version of the GCM. This technique has been shown to reproduce the non-local influence associated with the Eliassen and subsequent diabatic adjustments to the stratospheric forcings produced in the free running reference event (HH). Any potential spurious or missing sources of angular momentum are confined to the period when the stratospheric winds reverse (or immediately preceeding), prior to the main tropospheric response (Fig. 3). The method therefore captures tropospheric feedbacks associated with the zonal mean anomalies in the lower stratosphere; however, the strong zonal asymmetries associated with the displacement or splitting of the vortex during the reference event are not reproduced in the SSW ensemble.

The two SSW ensembles described here exhibit an annular-mode type response whose structure closely resembles the composite response to sudden warmings in the free running model, and in ERA-Interim. By experimental design, the tropospheric response is produced as a result of the stratospheric manifestation of the sudden warming, not though any purely tropospheric pathways. The strong resemblance between the SSW ensemble response and the

21

composite response in ERA Interim provides strong evidence that the downward influence implied by the dripping paint diagram of BD is real (issue 1 discussed in the introduction). Moreover, feedbacks involving tropospheric eddies at both planetary and synoptic scales play a significant role. Importantly, the timing of the tropospheric response in the SSW ensembles suggests that the most relevant aspect of the stratospheric variability is not the wind reversal in the mid-stratosphere, but the anomalies in the lower stratosphere, immediately above the troposphere.

The two ensembles also suggest that the intermittency or inconsistency of the tropospheric response (in the sense that during individual events the tropospheric jets can shift in the opposite direction to that favoured by the forcing) is likely a consequence of the signal to noise ratio (cf. issue 2). The mean response is of a similar order to the internal variability of the troposphere, and the magnitude and persistence of the intrinsic tropospheric variability is not strongly influenced by the stratospheric anomalies (Fig. 6).

The tropospheric response at longer timescales also does not depend strongly upon the strong stratospheric zonal asymmetries associated with whether the warming was a split or a displacement event (provided that the zonal mean anomalies are equally persistent). Since there are a number of limitations of this nudging technique at timescales of a week or two following the sudden warming, it does not preclude the relevance of these asymmetries on shorter timescales. Nor, given the limited statistical precision to which we know the observed response, does it rule out the possibility of higher order effects due to such asymmetries. However, at the timescales most relevant to seasonal forecasting, the observed response can be explained without invoking these effects.

Despite the fact that no asymmetries are explicitly induced in the stratosphere, the nudged ensembles exhibit a zonally asymmetric response that closely resembles that seen in composites of sudden warmings in the free running CMAM integration and in the ERA Interim reanalysis. This surface signature also strongly resembles the response described by Sigmond et al. (2013). The statistical robustness and causality implied by the experimental

22

design (both of which are absent from the observational record alone) lend strong confidence to the claim that this is a deterministic response to large-amplitude sudden warmings with an extended timescale recovery (cf. issue 3).

It must be stressed that the stratospheric anomalies in a real sudden warming are ultimately caused by planetary waves produced by the tropospheric flow. The downward influence in this sense is simply part of a causal chain of events, preceeded by the amplification of the planetary waves at the onset of the warming. Nonetheless, in the light of these results, a model which does not properly capture the structure of the stratospheric circulation anomalies during and following a sudden warming can not be expected to capture the tropospheric response. Nor would it capture the change in near surface circulation statistics implied by any secular change in the stratospheric polar vortex such as may be expected under an increase in well-mixed greenhouse gases. It is therefore of some concern that the near-surface, multi-model mean response of the CMIP-5 simulations is significantly weaker than that seen in the ERA Interim reanalysis composite. Whether the weak near-surface response seen in the CMIP-5 simulations is a result of deficiencies in stratospheric variability or of the tropospheric response, however, is not yet clear. The methodology introduced here provides a powerful tool for further investigating such questions, and, more generally, for clarifying the mechanisms underlying the coupling between the stratosphere and troposphere.

23

APPENDIX

Tropospheric response to the Nudging

The Coriolis acceleration induced by the stratospheric forcings is computed using the zonally symmetric quasi-geostrophic model on the sphere of Plumb (1982), which, solved for the residual vertical velocity gives

$$
\frac{\partial}{\partial z}\left(\frac{1}{\rho_0}\frac{\partial \rho_0 \overline{w}^*}{\partial z}\right) + \frac{N^2}{(2\Omega a)^2}\frac{\partial}{\partial \mu}\left(\frac{1-\mu^2}{\mu^2}\frac{\partial \overline{w}^*}{\partial \mu}\right)
$$

$$
= \frac{1}{2\Omega a}\frac{\partial}{\partial \mu}\left(\frac{\sqrt{1-\mu^2}}{\mu}\frac{\partial \mathcal{F} - k(z)u}{\partial z}\right) + \frac{H}{R}\frac{1}{(2\Omega a)^2}\frac{\partial}{\partial \mu}\left(\frac{1-\mu^2}{\mu^2}\frac{\partial Q - \alpha(z)T}{\partial \mu}\right),
$$

where $\mu = \sin\phi$. The lower boundary condition used is that of Haynes and Shepherd (1989); here the surface heat fluxes are assumed not to influence the lower boundary condition

$$
\frac{1}{\rho_0}\frac{\partial \rho_0 \overline{w}^*}{\partial z} - \frac{g}{4\Omega^2 a^2}\frac{\partial}{\partial \mu}\left(\frac{1-\mu^2}{\mu^2}\frac{\partial \overline{w}^*}{\partial \mu}\right) = 0.
$$

In the above, ρ_0 is the background density profile, Ω and a are the angular velocity and radius, respectively, of the Earth, R is the specific dry gas constant, H is the density scale height, and N^2 is the buoyancy frequency squared. The Rayeigh drag term is used to model surface friction and is set to $k(z) = \max(k_f(z - z_s)/z_s, 0)$ with $k_f = 2$ d^{-1} and $z_s = 1.5$ km, while the Newtonian cooling term represents the radiative terms and the analytical fit to the radiative timescales estimated to be relevant for the FREE run given in Hitchcock et al. (2013b) is used.

This equation is solved following the method described in the appendix of Hitchcock et al. (2013b). In this case the first 24 Hough modes are used to describe the meridional structure of the forcing, while a vertical domain from 0 to 100 km in log-pressure height is used at a vertical resolution of 50m. In all cases the global, DJF mean profile of N^2 from the FREE simulation is imposed. Stratospheric forcings are computed by applying a mask that ramps

linearly from zero at a lower pressure level p_b to one at an upper pressure level p_t; the results presented here use $p_b = 100$ hPa and $p_t = 50$ hPa, but they are not strongly dependant on these choices so long as p_b is above the tropopause. Note that the nudging itself is only active above 68 hPa. The momentum forcing $\mathcal{F}$ includes the resolved wave drag and all parameterized zonal momentum tendencies (including both orographic and non-orographic gravity wave drag and the zonal wind nudging tendencies). The thermodynamic forcing Q includes the thermodynamic nudging term alone.

REFERENCES

Alexandru, A., R. de Ella, R. Laprise, L. Separovic, and S. Biner, 2009: Sensitivity study of regional climate model simulations to large-scale nudging parameters. *Mon. Wea. Rev.*, **137**, 1666–1686, doi:10.1175/2008MWR2620.1.

Andrews, D. G., J. R. Holton, and C. B. Leovy, 1987: *Middle Atmosphere Dynamics*. Academic Press, London, UK.

Baldwin, M. P. and T. J. Dunkerton, 2001: Stratospheric harbingers of anomalous weather regimes. *Science*, **294**, 581–584, doi:10.1126/science.1063315.

Baldwin, M. P. and D. W. J. Thompson, 2009: A critical comparison of stratosphere–troposphere coupling indices. *Q. J. R. Meteorol. Soc.*, **135**, doi:10.1002/qj.479.

Bielli, S., H. Douville, and B. Pohl, 2010: Understanding the West African monsoon variability and its remote effects: an illustration of the grid point nudging methodology. *Clim. Dyn.*, **35**, 159–174, doi:10.1007/s00382-009-0667-8.

Charlton, A. J. and L. M. Polvani, 2007: A new look at stratospheric sudden warmings. Part I: Climatology and modelling benchmarks. *J. Clim.*, **20**, 449–469.

Charlton-Perez, A. J. and A. O'Neill, 2010: On the sensitivity of annular mode dynamics to stratospheric radiative timescales. *J. Clim.*, **23**, 476–484, doi:10.1175/2009JCLI2995.1.

Charlton-Perez, A. J., et al., 2013: On the lack of stratospheric dynamical variability in low-top versions of the cmip5 models. *J. Geophys. Res.*, **118**, 2494–2505, doi:10.1002/jgrd.50125.

Dee, D. P., et al., 2011: The ERA-Interim reanalysis: configuration and performance of the data assimilation system. *Q. J. R. Meteorol. Soc.*, **137**, 553–597, doi:10.1002/qj.828.

27

663 Domeisen, D., L. Sun, and G. Chen, 2013: The role of synoptic eddies in the tropospheric

664 response to stratospheric variability. *Geophys. Res. Lett.*, **40**, doi:10.1002/grl.50943.

665 Douville, H., 2009: Stratospheric polar vortex influence on Northern Hemisphere winter

666 climate variability. *Geophys. Res. Lett.*, **36**, L18 703, doi:10.1029/2009GL039334.

667 Gerber, E. P., C. Orbe, and L. M. Polvani, 2009: Stratospheric influence on the tropospheric

668 circulation revealed by idealized ensemble forecasts. *Geophys. Res. Lett.*, **36**, L24 801,

669 doi:10.1029/2009GL040913.

670 Gerber, E. P., et al., 2010: Stratosphere–troposphere coupling and annular mode variability

671 in chemistry-climate models. *J. Geophys. Res.*, **115**, D00M06, doi:10.1029/2009JD013770.

672 Haigh, J. D., M. Blackburn, and R. Day, 2005: The response of tropospheric circulation to

673 perturbations in lower-stratospheric temperature. *J. Clim.*, **18**, 3672–3685.

674 Hartley, D. E., J. T. Villarin, R. X. Black, and C. A. Davis, 1998: A new perspective on the

675 dynamical link between the stratosphere and troposphere. *Nature*, **391**, 471–474.

676 Haynes, P. H., C. J. Marks, M. E. McIntyre, T. G. Shepherd, and K. P. Shine, 1991: On

677 the "downward control" of extratropical diabatic circulations by eddy-induced mean zonal

678 forces. *J. Atmos. Sci.*, **48**, 651–678.

679 Haynes, P. H. and T. G. Shepherd, 1989: The importance of surface pressure changes in the

680 response of the atmosphere to zonally-symmetric thermal and mechanical forcing. *Q. J.*

681 *R. Meteorol. Soc.*, **115**, 1181–1208.

682 Hitchcock, P. and P. H. Haynes, in review: Zonally symmetric adjustment in the presence

683 of artificial relaxation. *J. Atmos. Sci.*

684 Hitchcock, P. and T. G. Shepherd, 2013: Zonal-mean dynamics of extended recoveries from

685 stratospheric sudden warmings. *J. Atmos. Sci.*, **70**, 688–707, doi:10.1175/JAS-D-12-0111.

686 1.

Hitchcock, P., T. G. Shepherd, and G. L. Manney, 2013a: Statistical characterization of Arctic Polar-night Jet Oscillation events. *J. Clim.*, **26**, 2096–2116, doi:10.1175/JCLI-D-12-00202.1.

Hitchcock, P., T. G. Shepherd, M. Taguchi, S. Yoden, and S. Noguchi, 2013b: Lower-stratospheric radiative damping and polar-night jet oscillation events. *J. Atmos. Sci.*, **70**, 1391–1408, doi:10.1175/JAS-D-12-0193.1.

Hoskins, B., R. Fonseca, M. Blackburn, and T. Jung, 2012: Relaxing the tropics to an observed state: analysis using a simple baroclinic model. *Q. J. R. Meteorol. Soc.*, **138**, 1618–1626, doi:10.1002/qj.1881.

Jung, T., M. J. Miller, and T. N. Palmer, 2010: Diagnosing the origin of extended-range forecast errors. *Mon. Wea. Rev.*, **138**, 2434–2446, doi:10.1175/2010MWR3255.1.

Martineau, P. and S.-W. Son, 2013: Planetary-scale wave activity as a source of varying tropospheric response to stratospheric sudden warming events: A case study. *J. Geophys. Res.*, **118**, doi:10.1002/jgrd.50871.

Matthewman, N. J. and J. G. Esler, 2011: Stratospheric sudden warmings as self-tuning resonances. part I: Vortex splitting events. *J. Atmos. Sci.*, **68**, 2481–2504, doi:10.1175/JAS-D-11-07.1.

Matthewman, N. J., J. G. Esler, A. J. Charlton-Perez, and L. M. Polvani, 2009: A new look at stratospheric sudden warmings. Part III: Polar vortex evolution and vertical structure. *J. Clim.*, **22**, 1566–1585, doi:10.1175/2008JCLI2365.1.

McLandress, C. and T. G. Shepherd, 2009: Impact of climate change on stratospheric sudden warmings as simulated by the Canadian Middle Atmosphere Model. *J. Clim.*, **22**, 5449–5463, doi:10.1175/2009JCLI3069.1.

Mitchell, D. M., L. J. Gray, J. Anstey, M. P. Baldwin, and A. J. Charlton-Perez, 2013: The influence of stratospheric vortex displacements and splits on surface climate. *J. Clim.*, **26**, 2668–2682, doi:10.1175/JCLI-D-12-00030.1.

Mudryk, L. R. and P. J. Kushner, 2011: A method to diagnose sources of annular mode time scales. *J. Geophys. Res.*, **116**, D14 114, doi:10.1029/2010JD015291.

Perlwitz, J. and N. Harnik, 2004: Downward coupling between the stratosphere and troposphere: The relative roles of wave and zonal mean processes. *J. Clim.*, **17**, 4902–4909, doi:10.1175/JCLI-3247.1.

Plumb, R. A., 1982: Zonally symmetric Hough modes and meridional circulations in the middle atmosphere. *J. Atmos. Sci.*, **39**, 983–991.

Plumb, R. A. and K. Semeniuk, 2003: Downward migration of extratropical zonal wind anomalies. *J. Geophys. Res.*, **108**, 4223, doi:10.1029/2002JD002773.

Polvani, L. M. and P. J. Kushner, 2002: Tropospheric response to stratospheric perturbations in a relatively simple general circulation model. *Geophys. Res. Lett.*, **29**, 1114, doi:10.1029/2001GL014284.

Reichler, T., J. Kim, E. Manzini, and J. Kröger, 2012: A stratospheric connection to Atlantic climate variability. *Nat. Geosci.*, **5**, 783–787, doi:10.1038/NGEO1586.

Scinocca, J. F., N. A. McFarlane, M. Lazare, J. Li, and D. Plummer, 2008: The CCCma third generation AGCM and its extension into the middle atmosphere. *Atmos. Chem. Phys.*, **8**, 7055–7074, doi:10.5194/acp-8-7055-2008.

Shaw, T. A., J. Perlwitz, and O. Weiner, 2014: Troposphere-stratosphere coupling: Links to north atlantic weather and climate, including their representation in CMIP5 models. *J. Geophys. Res.*, **119**, doi:10.1002/2013JD021191.

Shepherd, T. G., K. Semeniuk, and J. N. Koshyk, 1996: Sponge layer feedbacks in middle-atmosphere models. *J. Geophys. Res.*, **101**, 23 447–23 464.

Shepherd, T. G. and T. A. Shaw, 2004: The angular momentum constraint on climate sensitivity and downward influence in the middle atmosphere. *J. Atmos. Sci.*, **61**, 2899–2908.

Sigmond, M., J. F. Scinocca, V. V. Kharin, and T. G. Shepherd, 2013: Enhanced seasonal forecast skill following stratospheric sudden warmings. *Nat. Geosci.*, **6**, 98–102, doi:10. 1038/NGEO1698.

Simpson, I. R., M. Blackburn, and J. D. Haigh, 2009: The role of eddies in driving the tropospheric response to stratospheric heating perturbations. *J. Atmos. Sci.*, **66**, 1347–1365, doi:10.1175/2008JAS2758.1.

Simpson, I. R., P. Hitchcock, T. G. Shepherd, and J. F. Scinocca, 2011: Stratospheric variability and tropospheric annular-mode timescales. *Geophys. Res. Lett.*, **38**, L20 806, doi:10.1029/2011GL049304.

Simpson, I. R., P. Hitchcock, T. G. Shepherd, and J. F. Scinocca, 2013a: Southern Annular Mode dynamics in observations and models. Part I: The influence of climatological zonal wind biases in a comprehensive GCM. *J. Clim.*, **26**, 3953–3967, doi: 10.1175/JCLI-D-12-00348.1.

Simpson, I. R., T. G. Shepherd, P. Hitchcock, and J. F. Scinocca, 2013b: Southern Annular Mode dynamics in observations and models. Part II: Eddy feedbacks. *J. Clim.*, **26**, 5220–5241, doi:10.1175/JCLI-D-12-00495.1.

Song, Y. and W. A. Robinson, 2004: Dynamical mechanisms for stratospheric influences on the troposphere. *J. Atmos. Sci.*, **61**, 1711–1725.

756 Wittman, M. A. H., A. J. Charlton, and L. M. Polvani, 2007: The effect of lower stratospheric

757   shear on baroclinic instability. *J. Atmos. Sci.*, **64**, 479–496, doi:10.1175/JAS3828.1.

List of Tables

TABLE 1. Number of ensembles and sudden warming events for which a given field is availble from CMIP-5 and ERA-Interim data used for the composites of surface fields following sudden warming events. Extended winters (November through March) from the CMIP-5 historical runs from 1960/1961 to 2003/2004 were used and only the models for which there were more than 10 events in the available ensemble members were included in the composites. For ERA-Interim, winters from 1979/1980 to 2011/2012 were included.

Model	# ensembles		# warmings		warmings/dec
	T	U/V	T	U/V	
ACCESS1-0	1	-	12	-	2.8
CanESM2	5	5	231	231	10.7
CMCC-CMS	1	1	36	36	8.4
CNRM-CM5	1	1	18	18	4.2
GFDL-CM3	4	4	31	31	1.8
HadCM3	10	-	113	-	2.6
HadGEM2-CC	3	2	102	63	7.9
inmcm4	1	1	19	19	4.4
IPSL-CM5A-LR	4	4	75	75	4.4
IPSL-CM5A-MR	3	3	84	84	6.5
MIROC-ESM-CHEM	1	1	28	28	6.5
MIROC-ESM	3	3	87	87	6.7
MPI-ESM-LR	3	3	97	97	7.5
MPI-ESM-MR	2	2	67	67	7.8
MPI-ESM-P	1	1	27	27	6.3
NorESM1-M	3	-	29	-	2.2
ERA-Interim	1	1	22	22	6.7

List of Figures

35

789 5 NAM index in (a, c) the FREE event and in (b, d) the SSW composite for

790   (a, b) the displacement case and (c, d) the split case. Solid and dashed lines

791   in (b) and (d) as in Fig. 2. (e) Composite of NAM index following sudden

792   warmings in the FREE run. Gray shading in panels (b), (d), and (e) indicate

793   where the averages are not statistically different from zero at the 95% level.   42

794 6 (a) Histogram of the tropospheric NAM index at 500 hPa in CTRL and the

795   SSW ensembles. (b) Autocorrelations of the NAM at the same level for the

796   two cases. The 95% confidence intervals in (b) are estimated by computing

797   the autocorrelation function for each winter independently, and assuming the

798   sample mean is t-distributed. The time evolution of the 500 hPa NAM index

799   is shown in the thin grey lines for each ensemble member of (c) SSWd and

800   (d) SSWs. The bold lines show the ensemble means, the dashed lines indicate

801   the standard deviation, and the red and green lines show the 95% confidence

802   interval of a 22-member and 100-member ensemble, respectively, estimating

803   by sub-sampling with replacement.   43

804 7 Zonal mean zonal wind anomalies at 700 hPa (filled contours) and zonal mean

805   temperature anomalies at 200 hPa (contours, 1 K interval) in (a) the SSWd

806   ensemble and (b) the SSWs. (c, d) The same zonal wind anomalies projected

807   onto the leading EOF of the zonal wind at 700 hPa in the FREE event (using

808   data from December through May). (e, f) The difference between the full

809   anomaly field and the projection onto the leading EOF.   44

810 8 Vertical component of the anomalous EP flux, averaged in an area-weighted

811   sense from $50°$ to $90°$N, in (a) the SSWd ensemble and (b) the SSWs ensemble.

812   In both cases anomalies are defined relative to the CTRL integration.   45

9   (a, b) Planetary scale ($k = 1$ to 3) EP fluxes (filled contours) in the CTRL

run for January through March. Zonal mean zonal winds (contour lines) over

the same period, at intervals of 5 m s^{-1}. (c-f) Anomalous EP fluxes (filled

contours) during (c,d) 1-15 January and (e,f) February and March in the

SSWd ensemble. Zonal mean zonal wind anomalies (contour lines) over the

same periods at intervals of 0.5 m s^{-1} are also shown. (g,h) EP fluxes and

winds regressed against the NAM index at 300 hPa, scaled by the magnitude

of the FM NAM response in SSWd at 300 hPa (see text for details). Panels

(a,c,e,g) show the vertical component of the flux, while (b,d,f,h) show the

meridional component.   46

10   Same as Fig. 9 but for synoptic scale and smaller eddies ($k > 3$).   47

11   Composites of near surface temperature (left) and winds (right) for SSWs-

CTRL in (a,b) January and (c,d) February, and for SSWd-CTRL in (e,f)

January and (g,h) February. Shown in the left panels is the 2 m temperature,

and in the right panels the 10 m zonal wind (shading) and the surface wind

stress (vectors). The contours are the same as those in Fig. 1(b,c).   48

12   (a) Histogram of the monthly NAO index in CTRL and the SSW ensembles.

(b) Difference in the histograms for the SSW ensembles relative to CTRL.   49

13   Near surface (a) temperatures and (b) winds for the 30 days following a sudden

warming in the CMIP-5 multi-model mean composites. The filled contours

are as in Figs. 1 and 11. (c) Area-averaged temperatures for three regions

shown in the map for each CMIP-5 model in the multi-model ensemble, the

two SSW ensembles, and the ERA-Interim composite. Confidence intervals

(at 95%) are shown only for the SSW ensembles and ERA-Interim composite

for clarity. The multi-model mean response for each region is shown by the

dotted line.   50
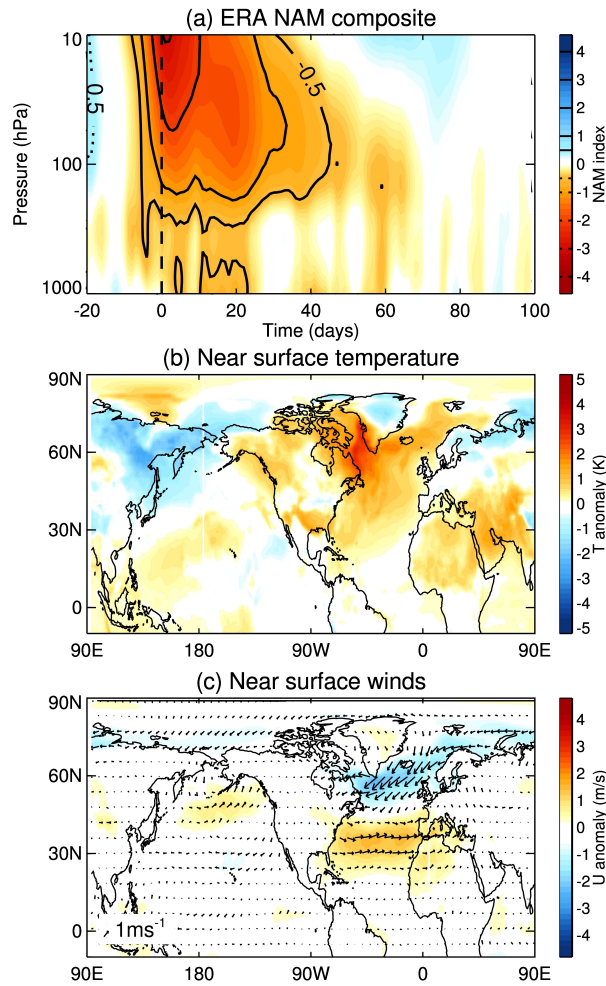
Fig. 1. (a) Composite of the NAM index following the 22 sudden warmings identified in the ERA Interim reanalysis in the 33 winters between 1979/1980 and 2011/2012. Composite of (b) 2 m temperature and (c) 10 m wind anomalies for the 30 days following the warmings. The shading in (c) shows the zonal component of the wind.
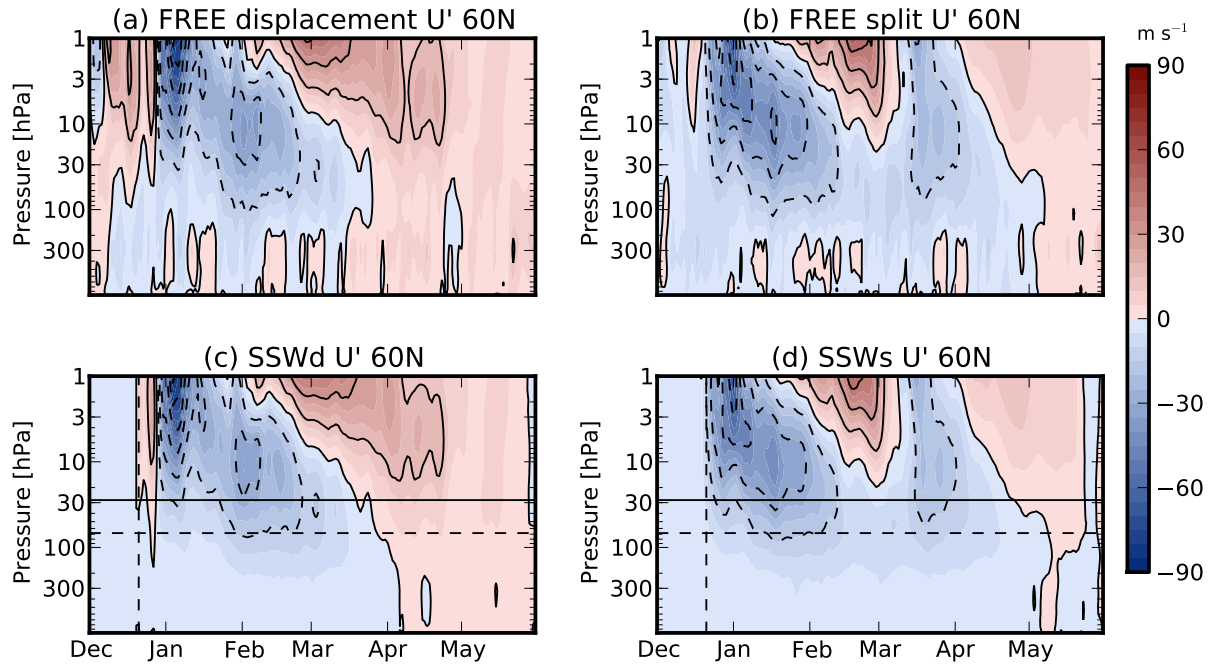
FIG. 2. Zonal mean zonal winds at 60°N in (a,b) the FREE reference events and (c,d) the SSW ensembles. The contours are at intervals of 10 m s⁻¹. In panels (c) and (d), the lower boundary of the nudging region is indicated by the dashed horizontal lines, and height at which the nudging reaches full strength by the solid horizontal lines. The reference date, 21 December, when the nudging in the SSW ensemble starts to force towards the instantaneous state of the FREE event, is indicated by the vertical lines.
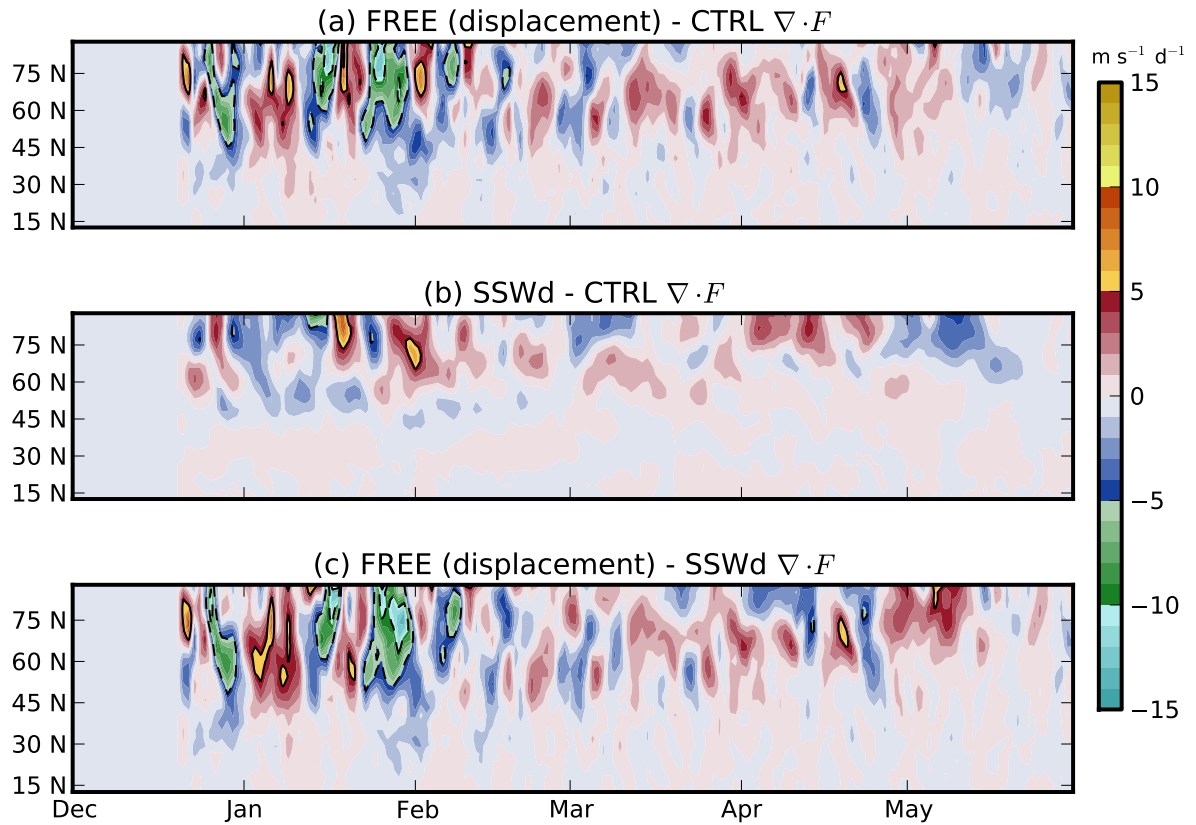
FIG. 3. Anomalous zonal mean wave driving (the acceleration due to EP Flux divergence of both resolved and unresolved waves) integrated in a mass-weighted sense from 100 hPa to 1 hPa, for (a) the FREE displacement event, (b) the SSW displacement ensemble and (c) the difference between the two. In (a) and (b) the anomalies are defined relative to the CTRL integration.
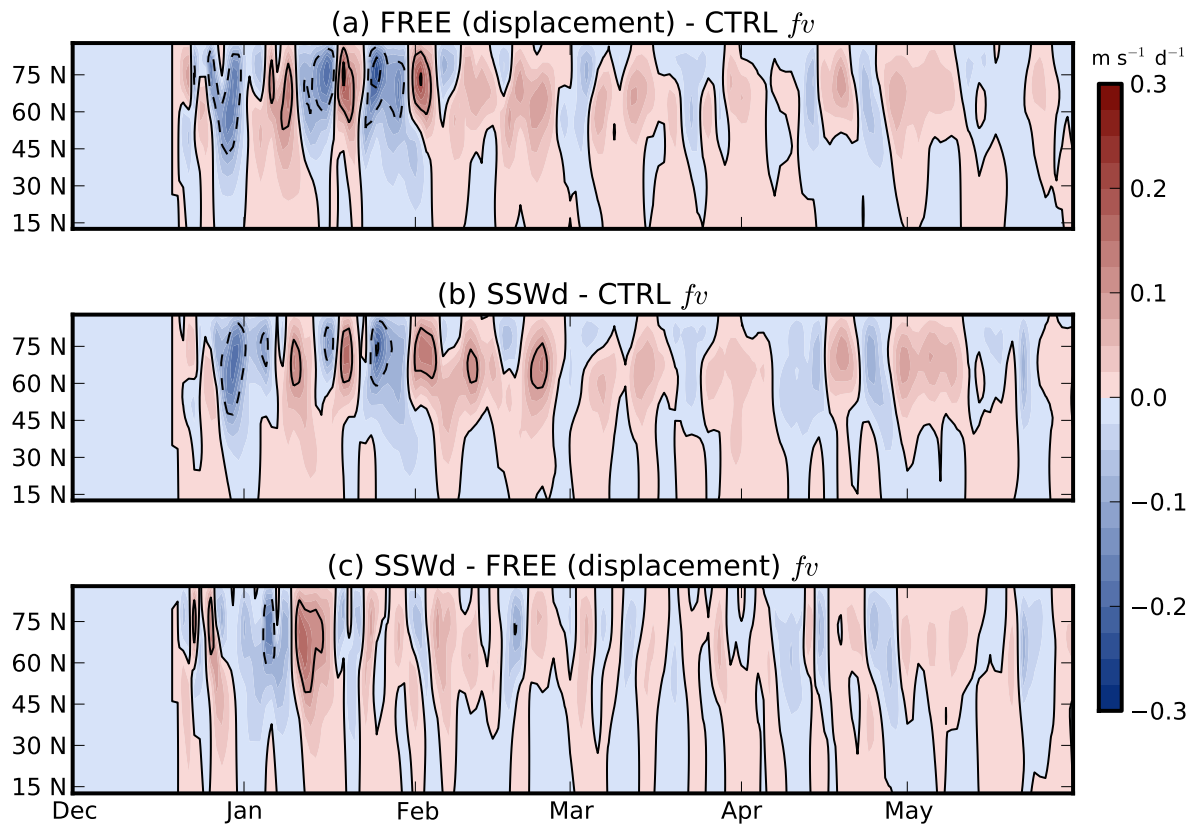
FIG. 4. Anomalous Coriolis accelerations (associated with the residual meridional velocity) induced by stratospheric forcings in (a) the FREE event, (b) the displacement SSW ensemble and (c) the difference between the two at 700 hPa. Contour intervals are 0.1 m s^{-1} d^{-1}. In (a) and (b) the anomalies are defined relative to the CTRL climatology.
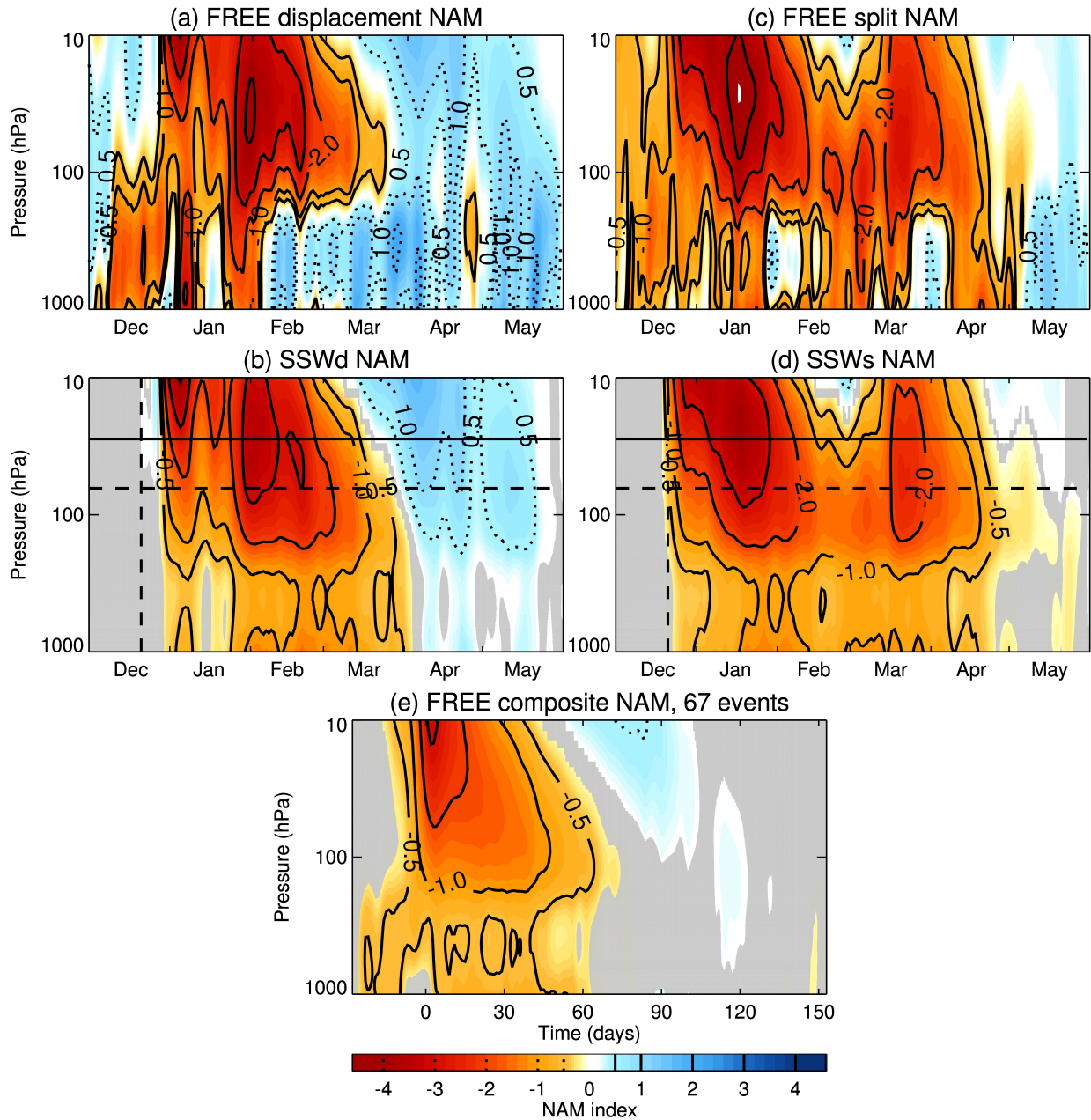
FIG. 5. NAM index in (a, c) the FREE event and in (b, d) the SSW composite for (a, b) the displacement case and (c, d) the split case. Solid and dashed lines in (b) and (d) as in Fig. 2. (e) Composite of NAM index following sudden warmings in the FREE run. Gray shading in panels (b), (d), and (e) indicate where the averages are not statistically different from zero at the 95% level.
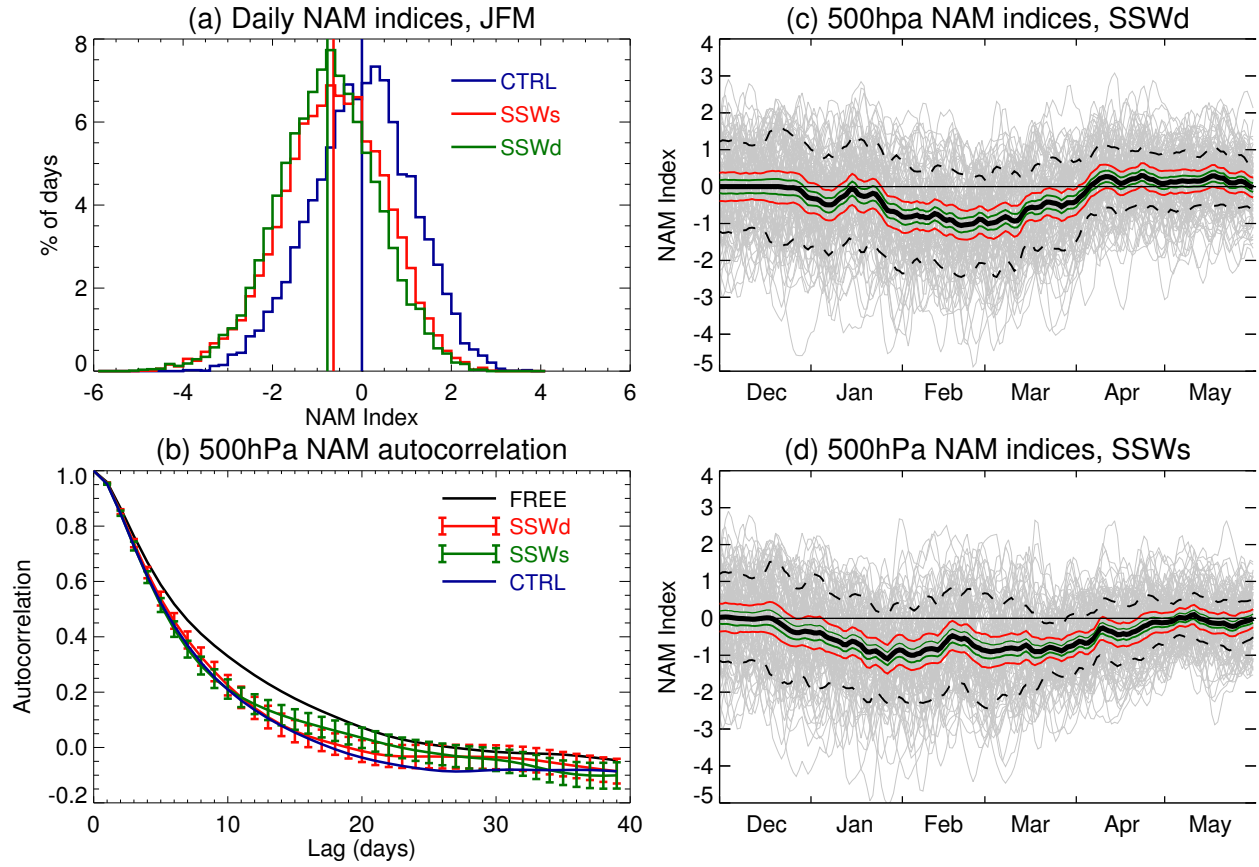
FIG. 6. (a) Histogram of the tropospheric NAM index at 500 hPa in CTRL and the SSW ensembles. (b) Autocorrelations of the NAM at the same level for the two cases. The 95% confidence intervals in (b) are estimated by computing the autocorrelation function for each winter independently, and assuming the sample mean is t-distributed. The time evolution of the 500 hPa NAM index is shown in the thin grey lines for each ensemble member of (c) SSWd and (d) SSWs. The bold lines show the ensemble means, the dashed lines indicate the standard deviation, and the red and green lines show the 95% confidence interval of a 22-member and 100-member ensemble, respectively, estimating by sub-sampling with replacement.
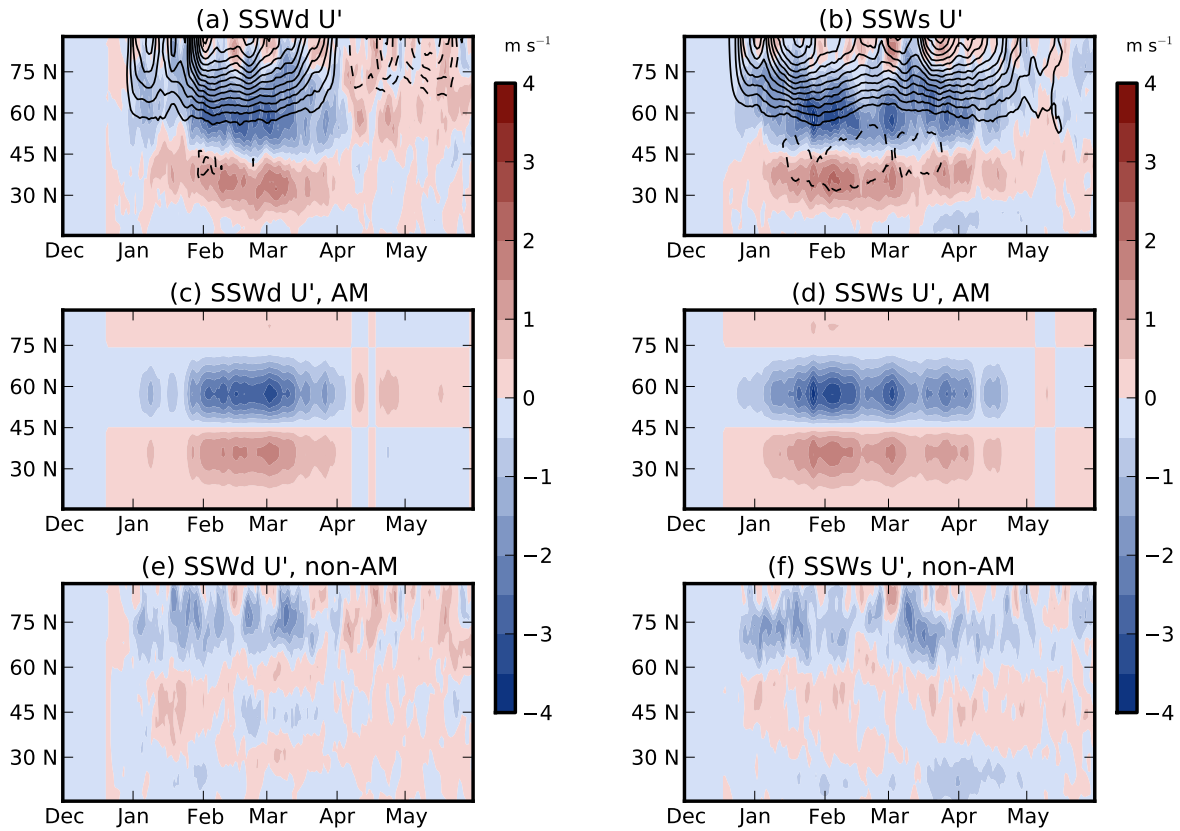
FIG. 7. Zonal mean zonal wind anomalies at 700 hPa (filled contours) and zonal mean temperature anomalies at 200 hPa (contours, 1 K interval) in (a) the SSWd ensemble and (b) the SSWs. (c, d) The same zonal wind anomalies projected onto the leading EOF of the zonal wind at 700 hPa in the FREE event (using data from December through May). (e, f) The difference between the full anomaly field and the projection onto the leading EOF.
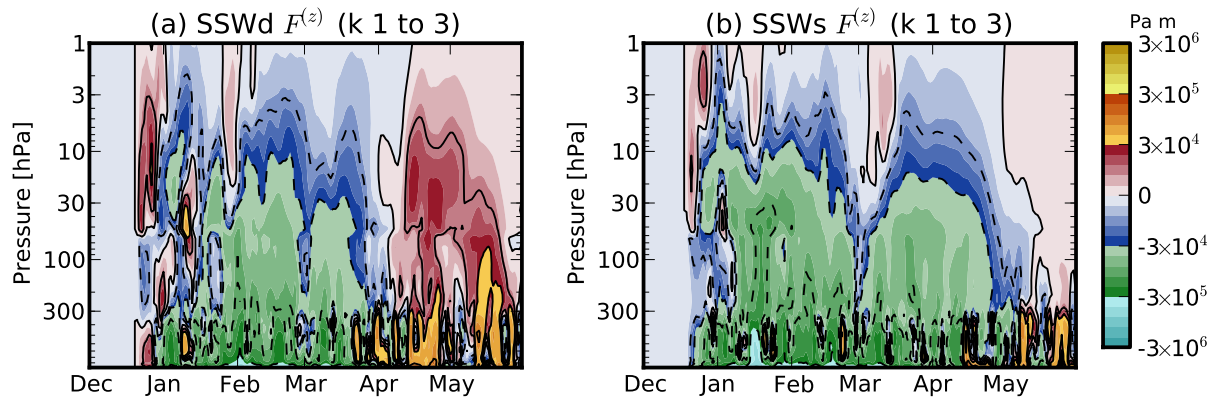
FIG. 8. Vertical component of the anomalous EP flux, averaged in an area-weighted sense from 50° to 90°N, in (a) the SSWd ensemble and (b) the SSWs ensemble. In both cases anomalies are defined relative to the CTRL integration.
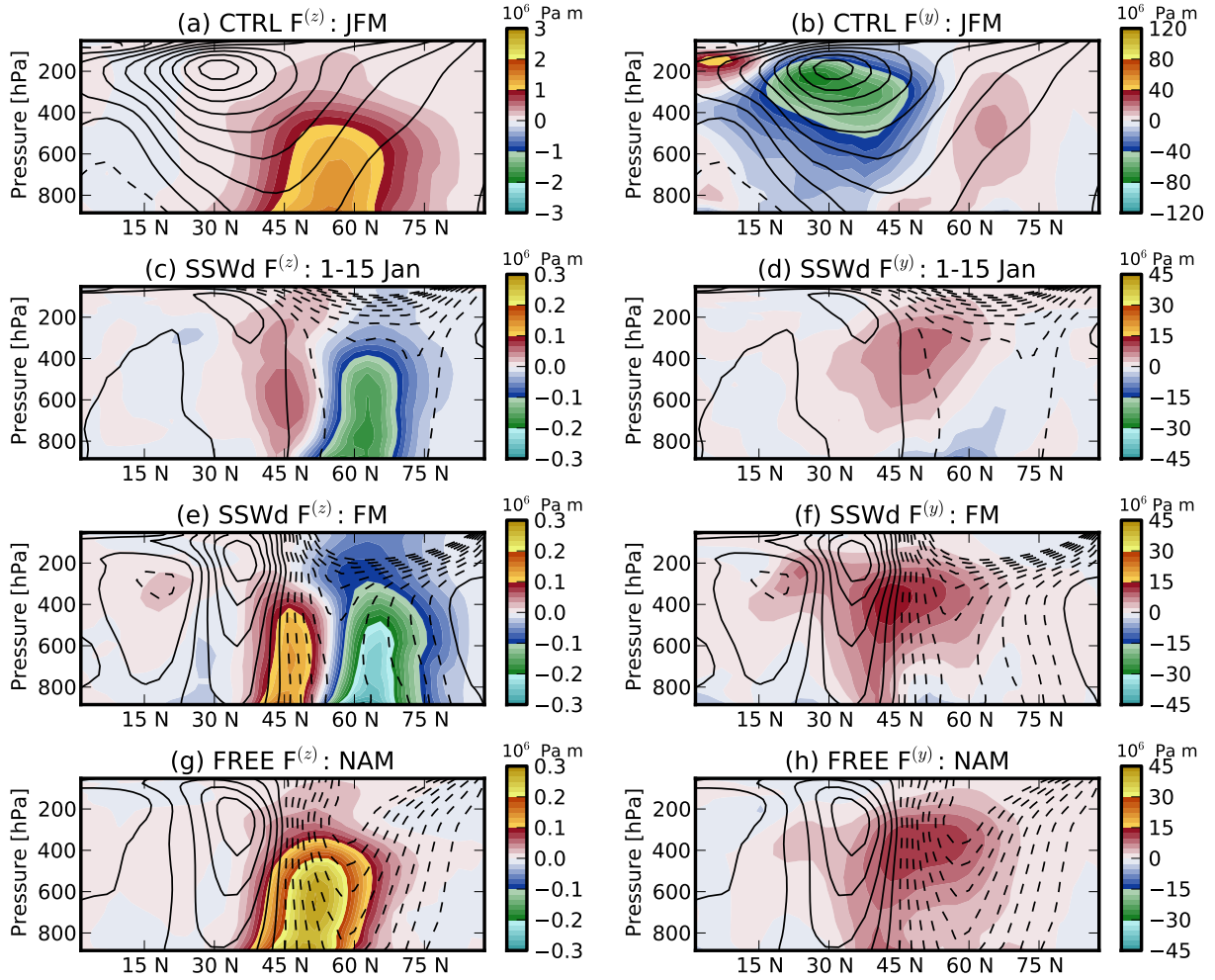
45

FIG. 9. (a, b) Planetary scale ($k = 1$ to 3) EP fluxes (filled contours) in the CTRL run for January through March. Zonal mean zonal winds (contour lines) over the same period, at intervals of 5 m s^{-1}. (c-f) Anomalous EP fluxes (filled contours) during (c,d) 1-15 January and (e,f) February and March in the SSWd ensemble. Zonal mean zonal wind anomalies (contour lines) over the same periods at intervals of 0.5 m s^{-1} are also shown. (g,h) EP fluxes and winds regressed against the NAM index at 300 hPa, scaled by the magnitude of the FM NAM response in SSWd at 300 hPa (see text for details). Panels (a,c,e,g) show the vertical component of the flux, while (b,d,f,h) show the meridional component.
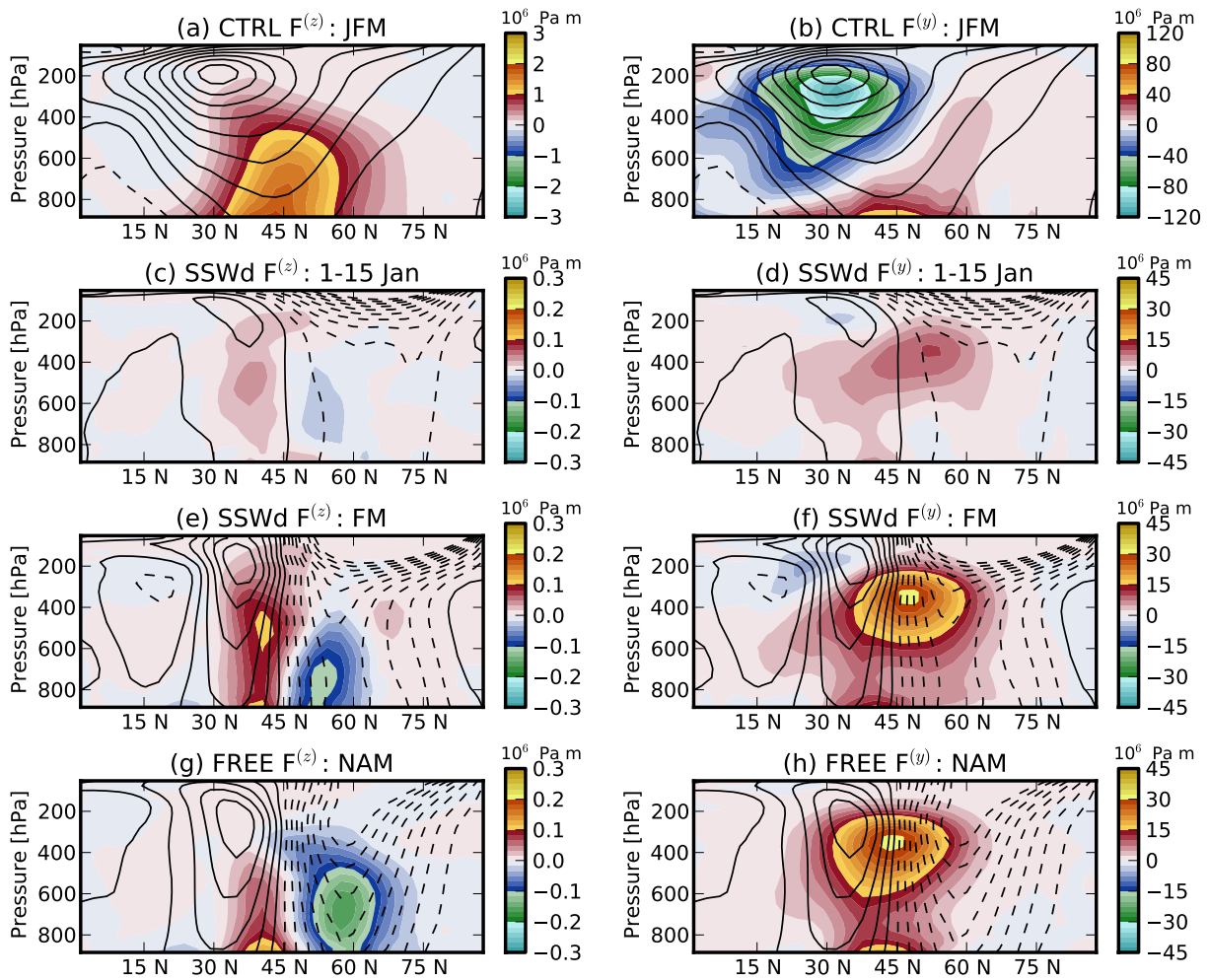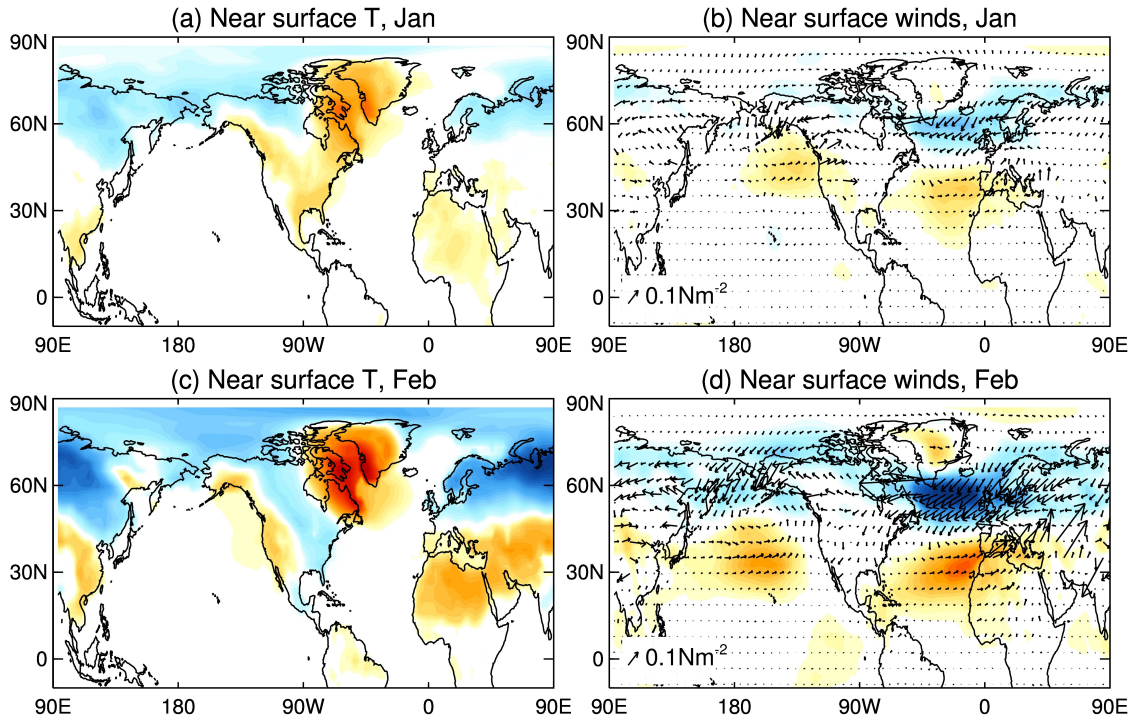
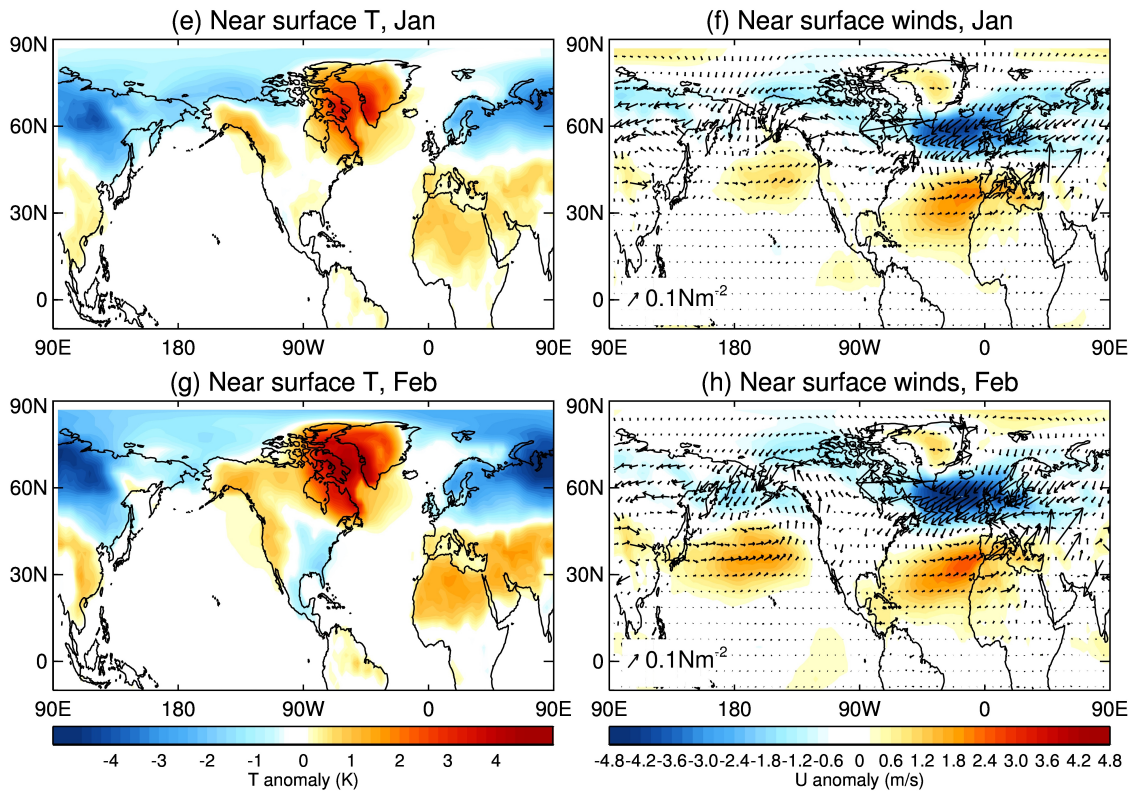Fig. 10. Same as Fig. 9 but for synoptic scale and smaller eddies ($k > 3$).

SSWs - CTRL

(a) Near surface T, Jan

(b) Near surface winds, Jan

(c) Near surface T, Feb

(d) Near surface winds, Feb

SSWd - CTRL

(e) Near surface T, Jan

(f) Near surface winds, Jan

(g) Near surface T, Feb

(h) Near surface winds, Feb

FIG. 11. Composites of near surface temperature (left) and winds (right) for SSWs-CTRL in (a,b) January and (c,d) February, and for SSWd-CTRL in (e,f) January and (g,h) February. Shown in the left panels is the 2 m temperature, and in the right panels the 10 m zonal wind (shading) and the surface wind stress (vectors). The contours are the same as those in Fig. 1(b,c).
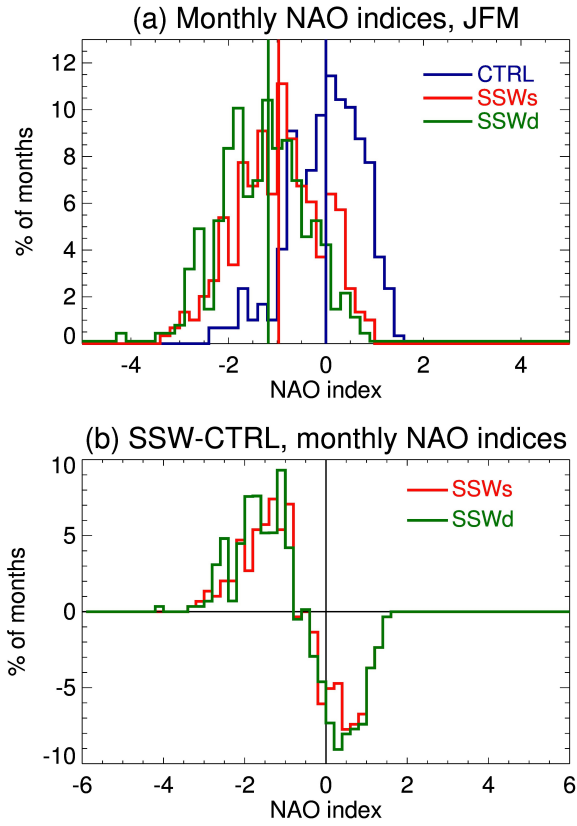
Fig. 12. (a) Histogram of the monthly NAO index in CTRL and the SSW ensembles. (b) Difference in the histograms for the SSW ensembles relative to CTRL.
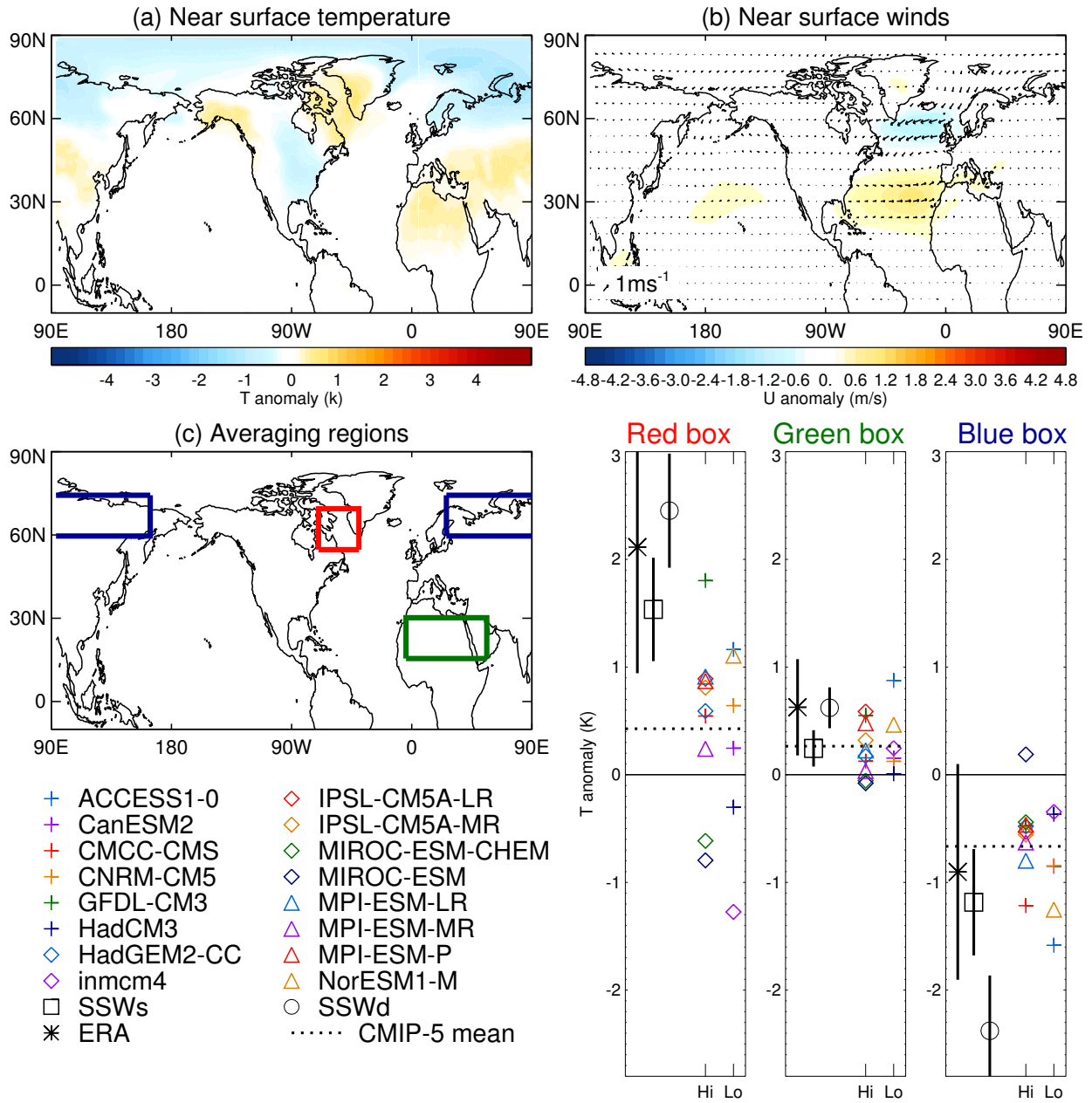
FIG. 13. Near surface (a) temperatures and (b) winds for the 30 days following a sudden warming in the CMIP-5 multi-model mean composites. The filled contours are as in Figs. 1 and 11. (c) Area-averaged temperatures for three regions shown in the map for each CMIP-5 model in the multi-model ensemble, the two SSW ensembles, and the ERA-Interim composite. Confidence intervals (at 95%) are shown only for the SSW ensembles and ERA-Interim composite for clarity. The multi-model mean response for each region is shown by the dotted line.